Available online at www.sciencedirect.com
SCIENCE DIRECT
Journal of volcanology and geothermal research
ELSEVIER
Journal of Volcanology and Geothermal Research 151 (2006) 279–307
www.elsevier.com/locate/jvolgeores

A submarine perspective of the Honolulu Volcanics, Oahu

David A. Clague [a,*], Jennifer B. Paduan [a], William C. McIntosh [b], Brian L. Cousens [c], Alicé S. Davis [a], Jennifer R. Reynolds [d]

[a] *Monterey Bay Aquarium Research Institute, 7700 Sandholdt Road, Moss Landing, CA 95039-9644, USA*
[b] *New Mexico Geochronology Research Laboratory, N.M. Bureau of Geology, New Mexico Tech, 801 Leroy Place, Socorro, 87801-4796, USA*
[c] *Ottawa-Carleton Geoscience Centre, Department of Earth Sciences, Carleton University, 1125 Colonel By Drive, Ottawa, Ontario, Canada K1S 5B6*
[d] *School of Fisheries and Ocean Sciences, West Coast and Polar Regions Undersea Research Center, University of Alaska Fairbanks, P.O. Box 757220, 213 O'Neill Building, Fairbanks, AK 99775, USA*

Accepted 15 July 2005
Available online 27 December 2005

Abstract

Lavas and volcaniclastic deposits were observed and collected from 4 submarine cones that are part of the Honolulu Volcanics on Oahu, Hawaii. The locations of these and a few additional, but unsampled, vents demonstrate that nearly all the vents are located on or very close to the shoreline of Oahu, with the most distal vent just 12 km offshore. The clastic samples and outcrops range from coarse breccias to cross-bedded ash deposits and show that explosive volcanism at depths between about 350 and 590 m depth played a part in forming these volcanic cones. The eruptive styles appear to be dominantly effusive to strombolian at greater depths, but apparently include violent phreatomagmatic explosive activity at the shallower sites along the submarine southwest extension of the Koko Rift. The compositions of the recovered samples are broadly similar to the strongly alkalic subaerial Honolulu Volcanics lavas, but the submarine lavas, erupted further from the Koolau caldera, have slightly more radiogenic Sr isotopic ratios, and trace element patterns that are distinct from either the subaerial Honolulu Volcanics or the submarine North Arch lavas. These patterns are characterized by moderate to strong positive Sr and P anomalies, and moderate to strong negative Cs, Rb, U, Th, Zr, and Hf anomalies. Most samples have strong negative K and moderate negative Ti anomalies, as do all subaerial Honolulu Volcanics and North Arch samples, but one group of samples from the Koko Rift lack this chemical signature. The data are consistent with more garnet in the source region for the off-shore samples than for either the on-shore Honolulu Volcanics lavas. New Ar–Ar ages show that eruptions at the submarine vents and Diamond Head occurred between about 0.5 Ma and 0.1 Ma, with the youngest ages from the Koko Rift. These ages are in general agreement with most published ages for the formation and suggest that some much younger ages reported previously from the Koko Rift are probably erroneously young.

Keywords: submarine volcanism; Hawaii; rejuvenated stage; Ar–Ar ages; radiogenic isotopes; trace elements; basalt petrogenesis

1. Introduction

The Honolulu Volcanics includes the famous landmark Diamond Head and the almost equally famous snorkeling site at Hanauma Bay on O'ahu's south coast, among 37 vents or groups of vents (Stearns and Vaksvik, 1935, 1938; Stearns, 1940; Winchell, 1947). The

* Corresponding author. Tel.: +1 831 775 1781; fax: +1 831 775 1620.
E-mail address: clague@mbari.org (D.A. Clague).

0377-0273/$ - see front matter © 2005 Elsevier B.V. All rights reserved.
doi:10.1016/j.jvolgeores.2005.07.036

formation has been studied extensively because of the large range of strongly alkalic compositions of the eruptive products (Clague and Frey, 1982; Yang et al., 2003), the abundant mantle xenoliths erupted at numerous vents (e.g. Jackson and Wright, 1970; Beeson and Jackson, 1971; Frey, 1980; Sen, 1988; Sen and Leeman, 1991) including Salt Lake Crater where spinel lherzolite and various garnet-bearing pyroxenite and lherzolite xenoliths occur in great abundance, and because many of the vents, particularly those close to the south shoreline, are tuff cones that formed during violent phreatomagmatic (Surtseyan) eruptions (Wentworth, 1926; Hay and Iijima, 1968; Moberly and Walker, 1987).

K–Ar ages reported for the Honolulu Volcanics range from 30 ka to 2.01 Ma (Funkhouser et al., 1968; Gramlich et al., 1972; Stearns and Dalrymple, 1978; Lanphere and Dalrymple, 1980; Ozawa et al., 2005), but many of the reported ages, particularly those ages >0.8 Ma, are deemed unreliable either because they are inconsistent with stratigraphic sequence or because ages determined for the same vent or flow are inconsistent. The variability of results has been attributed to the presence of excess argon trapped in xenocrysts or small fragments of mantle xenoliths in the lava samples (Lanphere and Dalrymple, 1980). The ages, and the field observation that the flows and cones erupted after deep erosion of the underlying Ko‘olau shield volcano, suggest that the eruptions forming the Honolulu Volcanics occurred significantly after the formation of the underlying subaerial shield, whose age is also poorly constrained at about 2.2–2.6 Ma (McDougall, 1964; Doell and Dalrymple, 1973). Haskins and Garcia (2004) suggest that the transition from early submarine shield lavas with Mauna Loa affinities to late shield lavas with typical high-SiO_2 Ko‘olau compositions took place about 2.9 Ma.

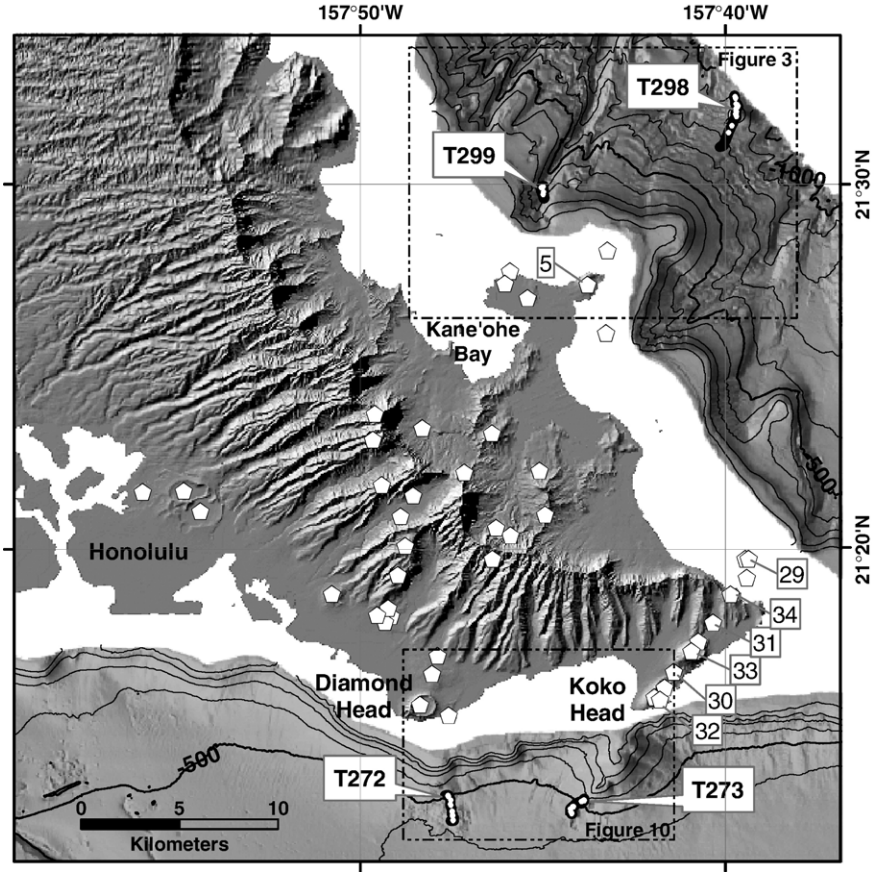

Fig. 1. Map of eastern O‘ahu with topography displayed as a sun-illuminated (from the northwest) image and offshore 30 kHz swath bathymetry (Dartnell and Gardner, 1999) shown as a slope-illuminated image with 100 m contours. The locations of the 37 known subaerial vents or groups of vents comprising the Honolulu Volcanics (Winchell, 1947; Jackson and Wright, 1970) are indicated by pentagons. The Koko Rift is the string of vents along the SE corner of O‘ahu. The four *ROV Tiburon* dives are labeled. Boxes indicate the locations of Figs. 3 and 10.

The Honolulu Volcanics ranges from alkalic basalt containing 46 wt.% SiO_2, through basanite and nephelinite, to nepheline melilitite containing as little as 35.5 wt.% SiO_2 (Clague and Frey, 1982). Many of the tuff cones, including Diamond Head, are of unknown composition because the ash samples are too weathered and zeolitized (Hay and Sheppard, 1977) to extract meaningful geochemical data although Winchell (1947) suggested that Diamond Head was nephelinite in composition based on petrography. The vents aligned along the Koko Rift (Kahauloa, Kalama, Koko Head-including the craters forming Hanauma Bay, Koko Crater, and Kaup) consist of alkalic basalt with the exception of Manana Island, which is nepheline melilitite (see summary in Clague and Frey, 1982). The range in compositions of the lavas has been attributed to variable degrees of partial melting of garnet-bearing lherzolite leaving residual apatite, phlogopite, and titanite at the smallest degrees of melting that produced the nepheline melilitites (Clague and Frey, 1982; Yang et al., 2003). The source has been inferred to be relatively homogeneous based on the small range in radiogenic isotopic ratios reported (Stille et al., 1983; Roden et al., 1984; Lassiter and Hauri, 1998). However, some details of the source characteristics have been difficult to determine due to significant mobility of many key trace elements during subaerial weathering and leaching (Clague and Frey, 1982; Yang et al., 2003).

High-resolution swath bathymetric and backscatter mapping of the region offshore from Koʻolau Volcano (Dartnell and Gardner, 1999) reveals several additional submarine vents of the Honolulu Volcanics, as well as hard (high-backscatter) substrate inferred to be lava flows on the south flank of Diamond Head. In 2001, we used the MBARI *R/V Western Flyer* and *ROV Tiburon* to conduct three dives on these recently mapped submarine cones and deposits of the Honolulu Volcanics and one dive in a canyon on the northeast side of Oʻahu (Fig. 1). Dive observations demonstrate that the submarine cones consist of lava flows and volcaniclastic deposits. Samples recovered during these dives include fresh glass, providing the first melt compositions for the Honolulu Volcanics, and samples for geochemical analysis and Ar–Ar dating. Data from these dives and samples allow us: (1) to evaluate the distribution of all the vents of the Honolulu Volcanics; (2) to determine the characteristics of these eruptions in shallow (<600 m) water; (3) to determine the age of several additional vents; and (4) to evaluate the homogeneity and characteristics of the mantle source of the magmas involved.

2. Analytical methods

Dive video was analyzed in context of the high-resolution bathymetric map data. Each dive was annotated for observed substrate and the results were then integrated with petrographic observations, glass compositions, and whole-rock compositions.

Fresh glass, found as sand grains and lapilli in volcaniclastic rocks and as individual sand grains sieved from push cores, was analyzed by electron microprobe with a JEOL Superprobe at the U.S. Geological Survey in Menlo Park using natural and synthetic standards. Methods and analytical precision and accuracy are described in Davis et al. (1994). A subset of the analytical data, selected to represent the range of compositions, is presented in Table 1.

Sixteen whole-rock lava samples from dives T298, T273, and T272 were analyzed for major and trace elements using a combination of XRF (X-ray fluorescence) and ICP-MS (inductively coupled plasma-mass spectrometry) techniques at the GeoAnalytical Laboratory at Washington State University (Table 2). Information on methods, precision, and accuracy for samples analyzed at this facility are available at http://www.wsu.edu/~geology/Pages/Services/Geolab.html. The whole-rock and glass analyses are plotted on a total alkalies versus silica diagram in Fig. 2.

Six lava samples, all analyzed for major and trace elements and representing 5 different compositions, were analyzed for Sr, Nd, and Pb isotopic ratios at Carleton University, Ontario using techniques outlined in the footnotes to Table 3, which also presents the analyses and analytical errors for the Sr and Nd isotopic data.

Three samples from the flank of Diamond Head (T272-R1, R6, and R11), 3 from the submarine southwest end of the Koko Rift (T273-R5, R6, and R9), and 2 from the cone northeast of Oʻahu (T298-R8 and R16) were analyzed using $^{40}Ar/^{39}Ar$ dating methods. Groundmass concentrates were prepared because electron microprobe observations showed that K was concentrated in the interstitial matrix in all eight samples. In samples from dives T272 and T273, the interstitial matrix contained variable but generally abundant interstitial glass, in some cases altered. In contrast, interstitial matrix in dive T298 samples appeared to be entirely crystallized and relatively unaltered. Groundmass concentrates were prepared using crushing, ultrasonic disaggregation, and Franz magnetic separation, hand

Table 1
Selected electron microprobe glass analyses. Final number following *R*ock samples is the number of analyzed grains averaged. Final number following *P*ush *C*ore samples is the number of the grain analyzed. High-Na_2O glass analyses are from Sen et al. (1996) for SL6-SMP, a melt phase within a xenolith from Salt Lake Crater, and Clague (unpublished data) for 88SAL1-4, a rind on a different Salt Lake Crater xenolith

Sample/analysis		SiO_2	TiO_2	Al_2O_3	FeO*	MnO	MgO	CaO	Na_2O	K_2O	P_2O_5	S	Cl	Total
Northeast cone—nephelinite														
298-R04	12	41.12	3.67	13.57	13.02	0.16	5.36	14.42	5.15	2.18	1.11	0.152	0.109	100.01
298-R10	5	40.90	3.61	14.36	12.81	0.22	4.98	13.49	5.26	2.37	1.30	0.164	0.115	99.56
298-R12	4	41.19	3.62	14.08	13.16	0.17	5.13	13.70	5.46	2.34	1.22	0.160	0.121	100.35
298-PC73	5	40.77	3.55	13.49	13.04	0.16	5.30	14.25	5.24	2.09	1.17	0.149	0.114	99.31
298-PC73	10	40.87	3.73	13.52	13.09	0.18	5.24	14.23	5.34	2.18	1.15	0.158	0.113	99.79
298-PC73	6	41.12	3.56	13.35	13.06	0.15	5.42	14.51	4.98	2.09	1.10	0.146	0.114	99.61
298-PC68	3	41.21	3.57	13.42	13.23	0.15	5.05	14.08	5.29	2.20	1.16	0.178	0.099	99.64
298-PC68	1	41.47	3.60	13.37	13.11	0.21	5.04	14.34	5.38	2.16	1.10	0.153	0.108	100.03
Northeast cone—alkalic basalt														
298-PC65	9	44.53	3.13	13.93	12.37	0.17	5.97	13.04	4.22	1.46	0.75	0.057	0.075	99.69
298-PC65	6	44.65	2.82	14.16	12.20	0.14	6.38	12.65	4.37	1.40	0.75	0.057	0.071	99.66
298-PC65	5	45.42	2.74	14.58	11.99	0.18	6.56	12.56	3.96	1.24	0.62	0.048	0.062	99.95
298-PC65	9	46.06	2.38	14.69	12.05	0.19	7.02	12.00	3.79	1.06	0.50	0.064	0.048	99.86
298-PC65	11	46.32	2.54	14.66	11.74	0.17	6.03	12.27	4.06	1.26	0.67	0.041	0.063	99.81
298-PC65	5	46.36	2.51	14.50	11.80	0.20	6.46	12.49	3.85	1.11	0.54	0.048	0.063	99.92
298-PC65	4	46.54	2.33	14.74	12.14	0.16	7.04	11.81	3.75	0.98	0.51	0.046	0.049	100.09
298-PC65	4	46.92	2.35	14.55	12.10	0.20	6.60	11.79	3.85	1.04	0.59	0.048	0.053	100.08
298-PC65	8	47.35	2.14	14.81	11.81	0.14	6.96	11.65	3.68	0.93	0.44	0.046	0.052	100.00
298-PC78	4	48.27	2.23	14.81	11.33	0.17	6.01	11.59	3.87	1.03	0.53	0.026	0.049	99.91
Northeast cone—tholeiitic basalt														
298-PC69	5	52.44	2.93	13.26	12.35	0.14	5.41	10.07	2.59	0.51	0.32	0.010	0.011	100.04
298-PC69	11	51.99	2.95	13.05	12.50	0.17	5.58	10.13	2.40	0.47	0.31	0.010	0.003	99.55
298-PC69	3	52.11	2.72	13.41	11.80	0.22	5.79	10.73	2.34	0.43	0.25	0.010	0.016	99.83
298-PC69	13	52.09	2.45	13.55	11.37	0.13	6.14	10.98	2.42	0.41	0.25	0.011	0.008	99.79
298-PC66	1	51.96	2.33	13.62	11.24	0.19	6.27	11.08	2.34	0.38	0.24	0.010	0.002	99.65
298-PC66	4	53.02	2.32	13.94	10.89	0.18	6.33	10.74	2.24	0.34	0.22	0.002	0.022	100.23
298-PC69	15	51.97	2.44	13.69	11.10	0.14	6.37	11.09	2.35	0.38	0.23	0.007	0.007	99.78
298-PC78	6	53.11	2.12	14.16	10.14	0.16	6.70	10.79	2.26	0.42	0.25	0.005	0.000	100.12
298-PC66	5	53.17	2.18	13.32	10.84	0.18	7.21	10.97	2.15	0.32	0.21	0.002	0.011	100.56
298-PC69	2	52.57	1.88	13.70	10.48	0.13	7.73	10.66	2.27	0.35	0.21	0.004	0.002	99.97
Koko Rift														
273-R03	8	47.68	2.23	15.46	11.74	0.19	5.87	12.03	3.16	0.80	0.33	0.067	0.023	99.58
273-R08	20	45.83	2.67	14.38	12.55	0.19	6.15	12.39	3.84	1.12	0.55	0.061	0.056	99.80
Diamond Head														
272-R03	10	46.12	2.61	14.68	12.73	0.16	6.22	12.37	3.85	1.11	0.53	0.071	0.061	100.51
272-PC63	3	46.61	2.62	15.13	11.91	0.17	5.31	12.76	3.96	1.13	0.58	0.062	0.059	100.27
272-PC63	7	46.13	2.49	14.72	12.20	0.19	5.92	12.37	3.82	1.05	0.49	0.066	0.073	99.60
272-PC63	2	46.47	2.52	14.55	12.16	0.19	6.16	12.29	3.79	1.05	0.51	0.072	0.052	99.81
272-PC63	6	45.81	2.55	14.52	12.22	0.14	6.33	12.37	3.86	1.11	0.53	0.087	0.056	99.72
272-PC63	12	46.75	2.46	14.87	12.18	0.18	6.38	12.02	3.59	0.94	0.44	0.058	0.049	100.01
272-PC63	8	46.64	2.54	14.87	12.37	0.15	6.41	12.14	3.70	1.03	0.45	0.060	0.050	100.48
272-PC63	2	46.25	2.52	14.69	12.13	0.20	6.46	11.96	3.62	0.99	0.47	0.067	0.047	99.51
272-PC63	3	45.44	2.61	14.05	11.37	0.14	7.46	14.49	2.96	0.91	0.50	0.049	0.061	100.12
Northeast canyon														
299-R03	4	40.79	2.41	15.38	13.14	0.21	4.56	13.68	6.81	1.69	1.51	0.144	0.141	100.46
High-Na_2O glasses														
SL6-SMP		45.27	2.70	20.81	7.29	0.19	3.05	7.81	8.31	3.06	–	–	–	98.49
88SAL1-4		48.16	1.95	18.96	8.10	0.26	2.82	6.23	8.23	2.62	1.09	0.057	–	98.47

picking, and, in some case, dilute HCl acid etching. The goal was to remove low-K plagioclase, pyroxene, and/or olivine phenocrysts from the higher K interstitial matrix and to remove or reduce authigenic clays. The groundmass concentrates were analyzed at the New Mexico Geochronology Research Laboratory using the resistance-furnace incremental heating method. The gas was extracted in 9 increments A to I at 575 (repeated), 650, 700, 750, 825, 925, 1025, 1200, and 1630 W. Abbreviated analytical methods are provided in the footnotes to Table 4, which summarizes the results. Age spectra, inverse isochron plots, complete analytical data, and detailed descriptions of the results for each sample provided by WCM are also posted at http://www.mbari.org/volcanism/HonoluluVolcMS/.

3. Cone on O‘ahu’s northeast flank

3.1. Morphology and dive observations

The newly identified offshore vents include a solitary cone off the northeast shore of O‘ahu where dive T298 was located (Fig. 3). The cone rises about 300 m above the regional slope to a minimum depth of 589 m. The cone is nearly symmetrical and has slopes of about 25° that increase towards the summit. A prominent, high-backscatter ridge extends to the southeast, in the upslope direction, and a less-defined high-backscatter ridge extends due north from the base of the cone. The dive began on this north-oriented ridge in pillow lavas (samples *R*ock 1 and R2; Fig. 4a), but quickly encountered fine bedded, eroded, volcaniclastic deposits that drape the lower flanks of the cone (R3, R4, R5; Fig. 4b). These deposits are only loosely consolidated and were also sampled using *P*ush-*C*ore 68 and PC73. The volcaniclastic deposits are increasingly coarser grained breccia towards the summit of the cone (Fig. 4c) and most samples collected from the upper slopes are basaltic clasts (R6, R7, R8, R9, and R11) from this breccia deposit (R10, and R12). The dive then crossed over the summit of the cone, which consists of blocky lava flows with few identifiable pillow lava shapes (R13-R16; Fig. 4d), before traversing down the south flank of the cone towards the south-southwest. The south flank mirrored the north side of the cone, with volcanic breccia deposits near the summit (R17) that contain basalt clasts (R18) and fining volcaniclastic deposits downslope.

3.2. Petrography

The samples from the cone are all nephelinite. Pillow samples R1 and R2 contain olivine and titanaugite microphenocrysts in a tachylite to fine crystalline matrix. Pillow rinds are altered to palagonite so that no glass remains. Titanaugite crystals are commonly sector-zoned and arranged in rosettes (Fig. 5g). These samples are moderately vesicular (10–15%) with open irregular vesicles up to about 2 mm across. Samples R3, R4, and R5 are volcanic sandstone to lapillistone (Fig. 6c) with dense to vesicular (to 40–50%) dark-brown glassy clasts in a matrix of fresh and altered glass, crystals, and tachylite fragments. The samples are variably altered with increasing amounts of palagonite from sample R3 to R4 to R5. The finer sand and silt matrix grains in R3 are mostly a different paler brown glass with only olivine microphenocysts. Similar grains are absent in R4 and rare in R5. These paler colored grains are part of slope-mantling deposits discussed in Section 6. Unconsolidated volcanic sands and lapilli recovered in PC65 and in PC73 and a loosely cemented clast from PC73 are similar in mineralogy, texture, and alteration to the darker brown lapilli in R3 to R5. Microphenocrysts of olivine in the clastic fragments are roughly the same size (<3 mm) as in the pillow lava samples, but titanaugite crystals are smaller and less abundant. Lava fragments collected from the volcanic breccia and from the summit are texturally similar to the samples collected from the pillows, except the vesicles are generally smaller and the groundmass of R8 and R16 is finely crystalline. Sample R11 contains olivine microphenocrysts that are surrounded by laths of titanaugite (Fig. 5h). Breccia sample R10 includes cm-sized irregular-shaped clasts with glass rinds on all sides, whereas sample R12 contains only a single unaltered glassy clast, the remainder is altered to bright orange–red palagonite (Fig. 6d). Breccia sample R17 contains unaltered glassy irregular clasts of highly vesicular basalt, but the sample is cemented by colorless clays and zeolites (Fig. 6e) and the matrix is completely altered except for the crystals of olivine and titanaugite.

3.3. Glass compositions

Glass from the northeast cone, with the exception of alkalic basalt sand grains in volcaniclastic rocks R3 and R5, is all nephelinite in composition (83 sand or lapilli analyses; Figs. 2 and 7, group A), although the grains vary from lower MgO (4.98 wt.%), lower CaO (13.5 wt.%), and higher Al_2O_3 (15.0 wt.%), Na_2O (5.6 wt.%), and K_2O (2.5 wt.%) to higher MgO (5.42 wt.%) and CaO (14.7 wt.%) with lower Al_2O_3 (13.25 wt.%), Na_2O (4.9 wt.%) and K_2O (2 wt.%) compositions. These glasses are high in S (average 1500 ppm), Cl (average 1100 ppm), TiO_2 (average 3.6 wt.%), FeO* (average 13

wt.%), K_2O (2.2 to 2.4 wt.%) and P_2O_5 (average 1.2 wt.%), but these elements do not have strong trends as a function of MgO content. The alkalic basalt glass fragments in R3 and R5 are described in Section 6.

3.4. Whole-rock chemistry

Six lava samples from the cone were analyzed (Table 2) and all are nephelinite in composition (Fig. 2). The lavas are relatively primitive, containing 12.3 to 12.9 wt.% MgO, and uniform in major element composition, with the exception of K_2O, which varies from 1.29 to 1.59 wt.%. The primitive mantle-normalized trace element data (Fig. 8) are consistent among the 6 samples and are strongly enriched in incompatible elements. The patterns are distinctive in having small negative Y, Ti, Hf, Zr, and Pb anomalies; large negative K, U, Th, Rb, and Cs anomalies; and small positive P and Sr anoma-

Table 2
Whole-rock analyses of submarine Honolulu Volcanics lavas. 273-R9 and 273-R12 were acid washed to remove secondary carbonate

Sample	272-R1	272-R6	272-R7	272-R9	272-R11	273-R1	273-R5	273-R6
SiO_2	44.93	44.85	45.15	45.31	45.27	46.52	46.36	46.20
TiO_2	2.24	2.23	2.27	1.98	1.95	1.89	1.94	1.86
Al_2O_3	12.34	12.34	12.49	12.64	12.70	13.47	13.62	13.47
FeO	12.55	13.02	12.12	12.12	11.95	11.95	12.12	12.05
MnO	0.19	0.18	0.19	0.19	0.19	0.18	0.17	0.18
MgO	12.24	12.33	12.23	11.63	12.23	11.66	11.25	11.98
CaO	11.07	11.07	11.21	11.37	11.08	10.42	10.83	10.63
Na_2O	2.67	2.70	2.64	2.84	2.75	2.65	2.53	2.53
K_2O	0.87	0.81	0.90	0.76	0.70	0.64	0.65	0.63
P_2O_5	0.38	0.39	0.40	0.45	0.44	0.28	0.30	0.28
Total	99.49	99.91	99.59	99.30	99.26	99.66	99.77	99.80
Trace element analyses (ppm)								
Ni	304	299	299	286	304	293	277	303
Cr	483	477	474	439	449	438	414	454
V	292	281	284	259	270	265	274	263
Ga	19	23	16	18	18	18	23	21
Cu	84	82	81	83	83	79	73	83
Zn	107	106	106	107	104	100	101	107
La	21.24	22.25	22.44	26.89	25.65	13.18	13.64	12.66
Ce	41.77	43.58	43.79	51.40	49.18	27.42	28.16	26.31
Pr	5.29	5.53	5.56	6.38	6.15	3.65	3.75	3.51
Nd	22.49	23.64	23.51	26.72	25.72	16.30	16.66	15.55
Sm	5.56	5.77	5.73	6.30	6.11	4.31	4.41	4.13
Eu	1.83	1.88	1.90	2.06	2.00	1.47	1.51	1.41
Gd	5.42	5.49	5.59	5.99	5.83	4.42	4.59	4.29
Tb	0.79	0.80	0.81	0.85	0.83	0.66	0.68	0.65
Dy	4.19	4.23	4.31	4.48	4.40	3.66	3.75	3.54
Ho	0.75	0.75	0.76	0.80	0.79	0.68	0.71	0.67
Er	1.85	1.86	1.90	1.96	1.94	1.74	1.80	1.72
Tm	0.24	0.24	0.25	0.26	0.25	0.24	0.24	0.23
Yb	1.40	1.39	1.45	1.50	1.49	1.40	1.45	1.40
Lu	0.21	0.21	0.21	0.22	0.22	0.22	0.22	0.22
Ba	340	343	359	374	344	254	265	248
Th	1.77	1.86	1.89	2.32	2.19	0.99	1.02	0.94
Nb	30.56	30.85	32.28	31.62	30.67	19.76	20.45	19.63
Y	20.78	20.41	21.81	22.41	22.19	19.02	19.60	19.30
Hf	2.97	2.97	3.02	2.76	2.73	2.36	2.45	2.29
Ta	1.90	1.92	1.93	1.76	1.69	1.24	1.27	1.21
U	0.47	0.52	0.50	0.62	0.58	0.32	0.30	0.34
Pb	1.32	1.38	1.37	1.79	1.70	0.90	0.92	0.87
Rb	20.9	19.6	22.2	17.9	16.4	15.7	12.1	12.3
Cs	0.27	0.46	0.29	0.26	0.23	0.18	0.16	0.17
Sr	516	515	540	609	589	427	476	442
Sc	24.3	22.1	25.3	24.8	24.0	24.3	26.0	26.5
Zr	111	108	115	106	105	84	87	84

Table 2 (*continued*)

Sample	273-R9	273-R12	298-R2	298-R6	298-R7	298-R8	298-R16	298-R18
SiO_2	43.31	42.37	41.08	40.79	41.22	41.02	41.21	40.31
TiO_2	2.16	2.16	3.16	3.09	3.13	3.16	3.15	3.16
Al_2O_3	12.31	12.35	11.02	10.78	10.89	11.07	11.04	10.91
FeO	12.59	12.84	13.74	14.07	13.82	13.91	13.50	14.04
MnO	0.20	0.20	0.18	0.19	0.20	0.19	0.19	0.19
MgO	12.66	12.74	12.79	12.90	12.65	12.29	12.56	12.63
CaO	11.06	10.96	12.12	11.91	12.00	12.15	12.12	12.21
Na_2O	2.76	2.72	3.66	3.85	3.72	3.89	3.68	3.61
K_2O	0.54	0.51	1.35	1.30	1.41	1.53	1.59	1.29
P_2O_5	0.52	0.53	0.89	0.87	0.88	0.89	0.90	0.91
Total	98.11	97.38	99.99	99.75	99.92	100.10	99.93	99.25
Trace element analyses								
Ni	259	254	293	307	291	268	282	288
Cr	458	455	523	539	535	522	516	521
V	267	260	340	303	323	318	320	325
Ga	18	17	22	22	20	21	21	22
Cu	71	82	72	78	74	63	79	74
Zn	114	116	132	131	130	129	138	131
La	28.11	28.52	51.41	50.88	50.79	51.90	52.44	51.53
Ce	54.26	54.61	99.08	97.98	97.88	100.07	101.39	99.43
Pr	6.78	6.85	12.35	12.21	12.20	12.50	12.59	12.44
Nd	28.39	28.46	51.20	50.25	50.28	51.47	51.79	51.08
Sm	6.73	6.72	11.46	11.17	11.18	11.48	11.48	11.45
Eu	2.21	2.19	3.50	3.41	3.45	3.47	3.52	3.48
Gd	6.36	6.36	9.69	9.48	9.52	9.61	9.75	9.78
Tb	0.90	0.89	1.23	1.21	1.21	1.22	1.24	1.24
Dy	4.65	4.64	5.78	5.66	5.66	5.80	5.85	5.90
Ho	0.81	0.81	0.89	0.88	0.89	0.92	0.92	0.91
Er	1.98	1.95	1.96	1.94	1.95	1.98	2.03	1.97
Tm	0.25	0.25	0.23	0.23	0.23	0.23	0.24	0.24
Yb	1.46	1.43	1.27	1.28	1.27	1.30	1.31	1.28
Lu	0.22	0.21	0.18	0.18	0.18	0.19	0.19	0.18
Ba	418	430	738	738	720	810	818	720
Th	2.49	2.50	4.31	4.23	4.25	4.33	4.37	4.34
Nb	34.50	34.77	71.83	70.95	71.93	66.60	74.09	66.45
Y	23.98	23.98	26.09	26.16	26.22	26.90	27.56	25.63
Hf	2.97	2.95	5.24	5.18	5.21	5.28	5.39	5.21
Ta	1.87	1.86	4.03	3.87	3.96	3.63	4.03	4.03
U	0.60	0.63	0.74	0.98	1.04	1.01	0.98	0.66
Pb	2.07	2.10	2.88	3.05	3.16	2.77	2.84	2.90
Rb	12.2	12.3	30.2	29.8	32.9	33.9	41.0	29.4
Cs	0.15	0.15	0.39	0.30	0.46	0.41	0.54	0.26
Sr	768	768	937	1031	1062	1101	985	962
Sc	26.7	25.1	22.2	24.7	23.7	24.2	24.7	19.0
Zr	120	119	226	229	228	233	239	219

lies. Several elements, particularly Cs, Rb, U, K, Pb, and Sr, are variable beyond analytical precision. These samples have more enriched light-REE and more depleted heavy-REE than any of the other samples.

3.5. Ar–Ar age data

The age spectrum for sample T298-R8 is slightly disturbed (Fig. 9a). Individual step errors are on the order of ± 0.1 Ma although radiogenic yields are somewhat higher than those of previous samples, ranging from about 2% to about 6%. K/Ca ratios reach 1.4 for the central part of the age spectrum, considerably higher than K/Ca ratios of samples from the other two localities, in keeping with higher K_2O contents of the whole-rock sample. The weighted mean age of steps B to G is 0.48 ± 0.10 Ma, with an MSWD (mean square of weighted deviates; York, 1969) value of 1.59, indicating that analytical error accounts for age variations among steps in this interval. The data form a fairly

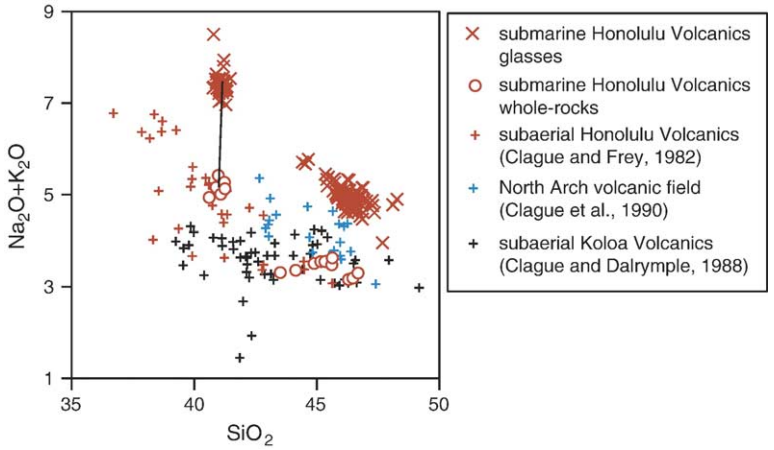

Fig. 2. Total alkalies versus silica diagram showing all the whole-rock and glass analyses for submarine samples from the Honolulu Volcanics. For comparison, whole-rock data for the subaerial Honolulu Volcanics (Clague and Frey, 1982) and Kōloa Volcanics (Clague and Dalrymple, 1988) and the submarine North Arch lava field (Clague et al., 1990) are plotted. The submarine Honolulu samples range from alkalic basalt to nephelinite.

tight cluster on an isotope correlation diagram, but fail to form a well-defined linear array. The intercept age (0.25 ± 0.18 Ma) has a large uncertainty, but overlaps with the weighted mean age.

The age spectrum of T298-R16 yielded relatively high quality results (Fig. 9b). K/Ca ratios are as high as 2.8 and radiogenic yields reach a maximum of more than 15%. The uncertainties of individual steps are on the order of ± 0.05 Ma, and the weighted mean age of concordant steps B to F is 0.52 ± 0.05 Ma (MSWD = 1.22). The data from these steps form a relatively well-defined linear array on an isotope correlation diagram, with an atmospheric $^{40}Ar/^{36}Ar$ intercept value (291 ± 10) and an intercept age that agrees closely with the weighted mean age (0.58 ± 0.14 Ma, MSWD = 1.3).

4. Cones on the submarine Koko Rift

4.1. Morphology and dive observations

The southwest submarine extension of the Koko Rift on the southeastern part of O'ahu consists of a series of irregularly shaped cones and an elongate ridge in a northeast–southwest direction where dive T273 explored the deeper two adjacent cones (Fig. 10) with the deepest cone rising about 110 m above the island slope to a summit at 427 m depth. The next cone to the northeast rises 110 m to a summit depth of 357 m. This small cone is perched on a sloping ridge with another small cone whose summit is at about 177 m depth. The shallowest, and easternmost, cone is broad and relative-

Table 3
Isotopic analyses

Sample	$^{208}Pb/^{204}Pb$	$^{207}Pb/^{204}Pb$	$^{206}Pb/^{204}Pb$	$^{87}Sr/^{86}Sr$	2σ	$^{144}Nd/^{143}Nd$	2σ
T272-R7	38.001	15.541	18.242	0.703451	10	0.513075	4
T272-R9	37.509	15.349	18.021	0.703378*	20	0.513075	16
T273-R1	37.759	15.462	18.116	0.703467	11	0.513070	4
T273-R12	37.708	15.431	18.094	0.703426	12	0.513067	5
T298-R16	37.652	15.419	18.002	0.703633	17	0.513002	10
				0.703414*	8		
T298-R18	37.695	15.432	18.020	0.703624	14	0.513041	15
				0.703375*	9		

Determined at Carleton University utilizing techniques described in Cousens (1996) on a Finnigan MAT261 multicollector mass spectrometer running in static mode. Nd isotope ratios are normalized to $^{146}Nd/^{144}Nd = 0.72190$. 67 runs of the La Jolla standard average $^{143}Nd/^{144}Nd = 0.511876 \pm 18$ (2σ, September 1992–December 1999). Sr isotope ratios are normalized to $^{86}Sr/^{88}Sr = 0.11940$ to correct for fractionation. Two Sr standards are run at Carleton, NIST SRM987 ($^{87}Sr/^{86}Sr = 0.710251 \pm 18$, n = 50, September 1992–December 1999) and the Eimer and Amend (E&A) $SrCO_3$ ($^{87}Sr/^{86}Sr = 0.708032 \pm 25$, n = 22, September 1994–December 1999). All Pb mass spectrometer runs are corrected for fractionation using NIST SRM981. The average ratios measured for SRM981 are $^{206}Pb/^{204}Pb = 16.890 \pm 0.012$, $^{207}Pb/^{204}Pb = 15.429 \pm 0.014$, and $^{208}Pb/^{204}Pb = 36.502 \pm 0.048$ (2σ), based on 73 runs from September 1992–December 1999. The fractionation correction is +0.13%/amu based on accepted values of Todt et al. (1984). Samples with * were leached for 24 h in 2N HCl at 125 °C and then kept at room temperature for 4 days; all others leached for 3 h in warm 2N HCl.

Table 4
Summary of $^{40}Ar/^{39}Ar$ results

Sample	Unit	Lab #	Sample wt.	*n*%	^{39}Ar	MSWD	K/Ca	Age (Ma)	$\pm 2\sigma$
T272-R1	Diamond Head	53245-01	159.9 mg	6	57.9	1.32	0.4	**0.36**	**0.07**
T272-R6	Diamond Head	53244-01	159.0 mg	6	65.2	3.16	0.2	0.81	0.62
T272-R11	Diamond Head	53240-01	164.1 mg	3	55.4	0.97	0.2	−0.43	0.63
T273-R5	Koko Rift	53265-01	159.0 mg	5	84.9	4.00	0.2	**0.14**	**0.10**
T273-R6	Koko Rift	53241-01	162.5 mg	4	72.4	0.66	0.2	**0.14**	**0.06**
T273-R9	Koko Rift	53242-01	162.3 mg	6	58.4	0.87	0.2	0.06	0.05
Mean	**Koko Rift**							**0.14**	**0.05**
T298-R8	NE Cone	53243-01	161.1 mg	6	73.9	1.59	0.9	**0.48**	**0.10**
T298-R16	NE Cone	53246-01	161.3 mg	5	69.9	1.22	2.0	**0.52**	**0.05**
Mean	**NE Cone**			**2**				**0.51**	**0.04**

Age determinations shown in bold are considered more reliable.

Sample preparation and irradiation: Groundmass concentrates were prepared using crushing, dilute HCl acid treatment, Franz magnetic separator, and hand-picking techniques. Groundmass concentrates were loaded into a machined Al disc and irradiated for 1 hour in the D-3 position, Nuclear Science Center, College Station, TX. Neutron flux monitor Fish Canyon Tuff sanidine (FC-1) equivalent to Mmhb-1 at 520.4 Ma (Samson and Alexander, 1987). Assigned age = 27.84 Ma (Deino and Potts, 1990).

Instrumentation: Mass Analyzer Products 215-50 mass spectrometer on line with automated all-metal extraction system. Separate was step-heated using a Mo double-vacuum resistance furnace. Heating duration in the furnace was 10 min. Reactive gases removed during furnace analysis by reaction with 3 SAES GP-50 getters, 2 operated at ~450 °C and 1 at 20 °C. Gas also exposed to a W filament operated at ~2000 °C.

Analytical parameters: Electron multiplier sensitivity averaged 2.09×10^{-16} mol/pA. Total system blank and background for the furnace averaged 2100, 8.1, 2.2, 42, 9.0×10^{-18} mol. J-factors determined to a precision of ±0.1% by CO_2 laser-fusion of 4 single crystals from each of 4 radial positions around the irradiation tray or 4 radial positions at two heights for encapsulation tubes. Correction factors for interfering nuclear reactions determined using K-glass and CaF_2 are as follows: $(^{40}Ar/^{39}Ar)_K = 0.0002 \pm 0.0003$; $(^{36}Ar/^{37}Ar)_{Ca} = 0.00028 \pm 0.000005$; and $(^{39}Ar/^{37}Ar)_{Ca} = 0.00072 \pm 0.00002$.

Age calculations: Plateau age or preferred age calculated for the indicated steps by weighting each step by the inverse of the variance. Plateau age error is inverse-variance-weighted mean error (Taylor, 1982) times root MSWD where MSWD > 1. MSWD values are calculated for $n - 1$ degrees of freedom for plateau age. Isochron ages, $^{40}Ar/^{36}Ar_i$ and MSWD values calculated from regression results obtained by the methods of York (1969). Decay constants and isotopic abundances after Steiger and Jäger (1977). All errors reported at $\pm 2\sigma$.

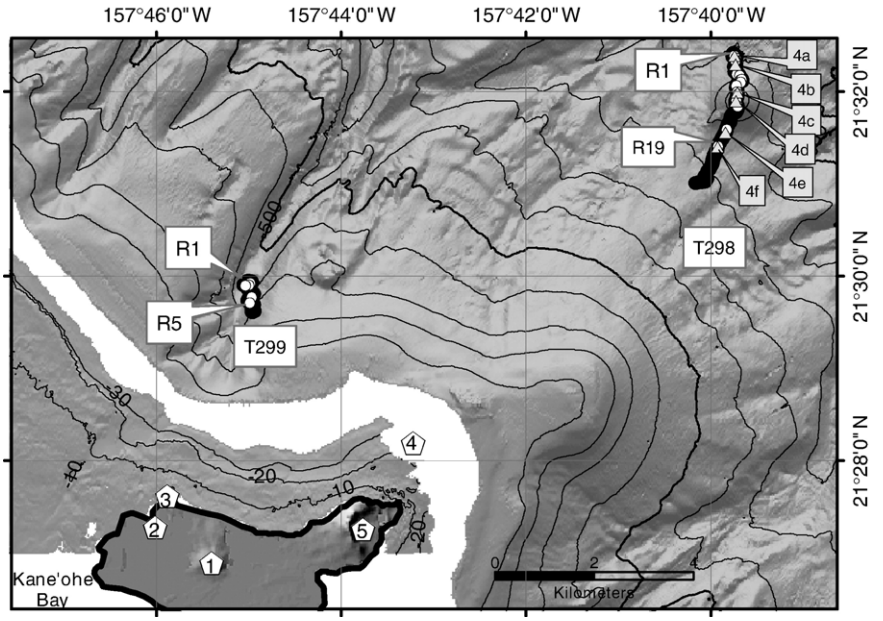

Fig. 3. Map showing the region on the northwest side of O'ahu and the dive tracks for *ROV Tiburon* dives T298 and T299. The known subaerial vents of the Honolulu Volcanics are shown as pentagons labeled with vent group numbers (smallest numbers are inferred to be oldest Honolulu Volcanics vents) from Jackson and Wright (1970). Offshore bathymetry as in Fig. 1 with additional nearshore Lidar data (U.S. Army Corps of Engineers, Mobile, Alabama, http://shoals.sam.usace.army.mil/default.htm). The locations of the bottom photographs in this figure are indicated along the track of dive T298, as are the first and last rock sample collected during the dive.

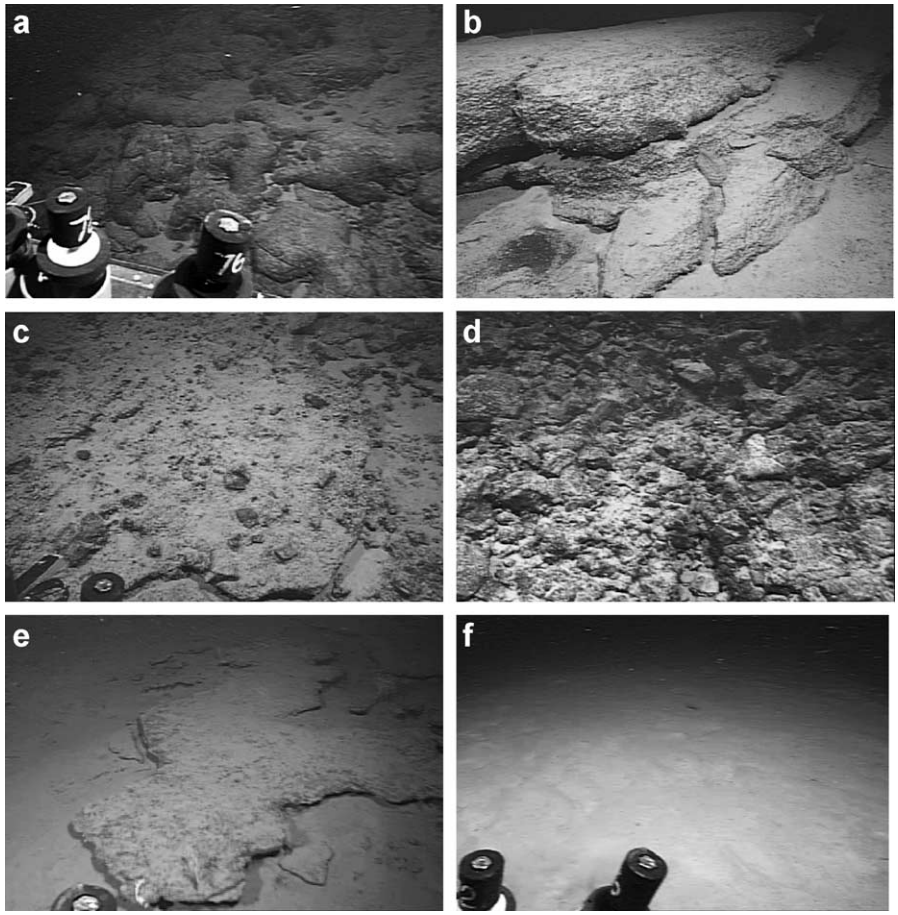

Fig. 4. Framegrabs of video recorded during *ROV Tiburon* dive T298. Each image shows an area of the seafloor roughly 3–4 m across. (a) Pillow basalt near collection site of *R*ock-1 at 868 m, (b) volcaniclastite deposits near collection sites for R-3 to R-5 at 863 m, (c) coarse volcanic breccia similar to collection sites of R-10 to R-12 at 668 m, (d) blocky lava flows at summit of cone at 589 m, (e) thin-bedded volcaniclastite deposits near collection site of R-19 at 832 m, (f) rippled sediment at end of dive near *P*ush*C*ore-66 and PC69 at 830 m.

ly flat-topped with the summit <100 m deep. The top is complex and may represent several nested cones and craters, subsequently eroded and smoothed during at least the last Pleistocene glacial period when the summit of this cone was emergent. The deeper, steep cones all have high backscatter, whereas the shallowest cone has irregular moderate backscatter.

The deeper westernmost cone consists of bedded fine-grained volcaniclastic deposits (R3, R4, and R8) with a veneer of angular basalt talus (R1, R2, and R5) and thin discontinuous unconsolidated sediment (Fig. 11a). The distribution of the talus is patchy with some areas entirely covered and others with virtually none. Towards the top of the westernmost cone, in-place pillow lava (R6 and R7; Fig. 11b), presumably the source of the talus observed downslope, was observed on top of the volcaniclastic deposits. In several places the volcaniclastic deposits are strongly laminated and display cross-bedding (R8; Fig. 11c). The small cone directly to the east also consisted of volcaniclastic deposits with loose talus fragments of basalt (R9 to R13) scattered on the surface.

4.2. Petrography

The samples from the two cones have different petrography with the lava samples from the southwestern deeper cone (R1, R2, R5, R6, and R7) having microphenocrysts of olivine and plagioclase and those from the northeastern cone (R9 to R13) having microphenocrysts of olivine and augite. The lava samples from both cones are moderately (20%) to highly (60%) vesicular and many have calcite filling or partly filling the vesicles.

The volcaniclastic samples from the southwestern cone (R3 and R4) have olivine plus plagioclase microphenocrysts, like the lava samples from the same cone, whereas the sample from the saddle (R8) between the two cones has the mineralogy of the eastern cone. The

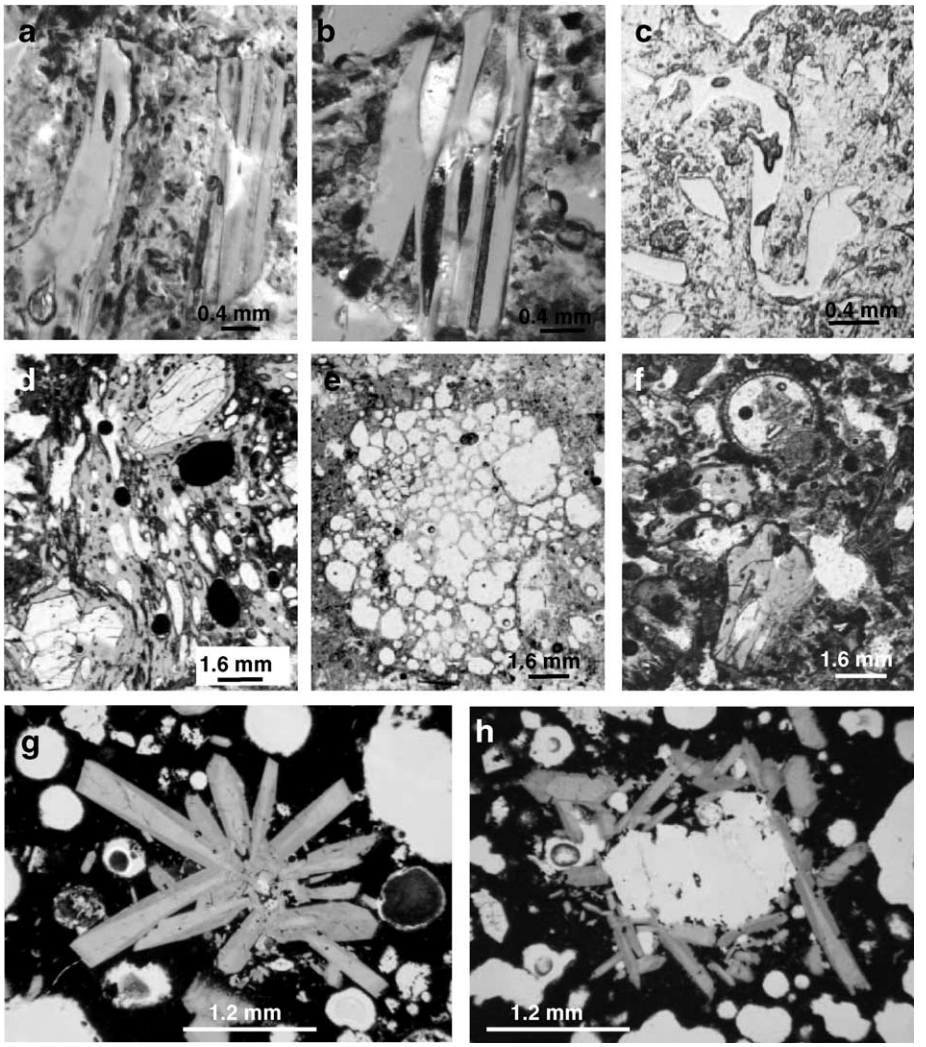

Fig. 5. Photomicrographs of samples from dives T272, T273, and T298. Images are in plane light unless otherwise indicated. (a) and (b) Stretched vesicular pyroclasts in T272-R4; (c) fluidal pyroclast in T273-R8, reflected light; (d) fluidal vesicular lapillus containing olivine phenocrysts in T298-R19; (e) highly vesicular lapillus in T298-R19; (f) glass grain (center bottom) adjacent to round foraminifer (center top) in T298-R19; (g) stellate cluster of sector-zoned titanaugite crystals in sample T298-R1, a characteristic of nephelinite comprising cone explored during dive T298; (h) olivine phenocryst surrounded by elongate titanaugite crystals in sample T298-R11, another petrographic characteristic of the nephelinite comprising the cone explored during dive T298.

volcaniclastic samples R3 and R4 are sandstones to lapillistones with irregular vesicular to dense glass shards (Fig. 6b) that in the case of R3 are completely altered to palagonite. Sample R8 is a graded volcanic siltstone to sandstone that displays cross-bedding. Glass shards and angular vesicular fragments are best preserved in the coarser sand layers and include fluidal shapes (Fig. 5c).

4.3. Glass compositions

The 26 glass analyses (all from R3 and R8) from the two cones on the Koko Rift define two alkalic basalt compositions (Table 1) that are most likely representative of the two cones, although R8 was collected from the saddle between the cones (Fig. 7, group D includes both compositions). The higher-SiO_2 composition also has higher Al_2O_3, and lower TiO_2, FeO, CaO, Na_2O, K_2O, P_2O_5 and is from the deeper cone. These glasses have low MgO contents (5.76 to 6.31 wt.%) and intermediate S contents (440 to 920 ppm) with a broad trend of increasing S with decreasing SiO_2 (Fig. 12). Except for their elevated S content caused by their submarine eruption, these alkalic basalts are similar in composition to alkalic basalt that characterizes the subaerial Koko Rift.

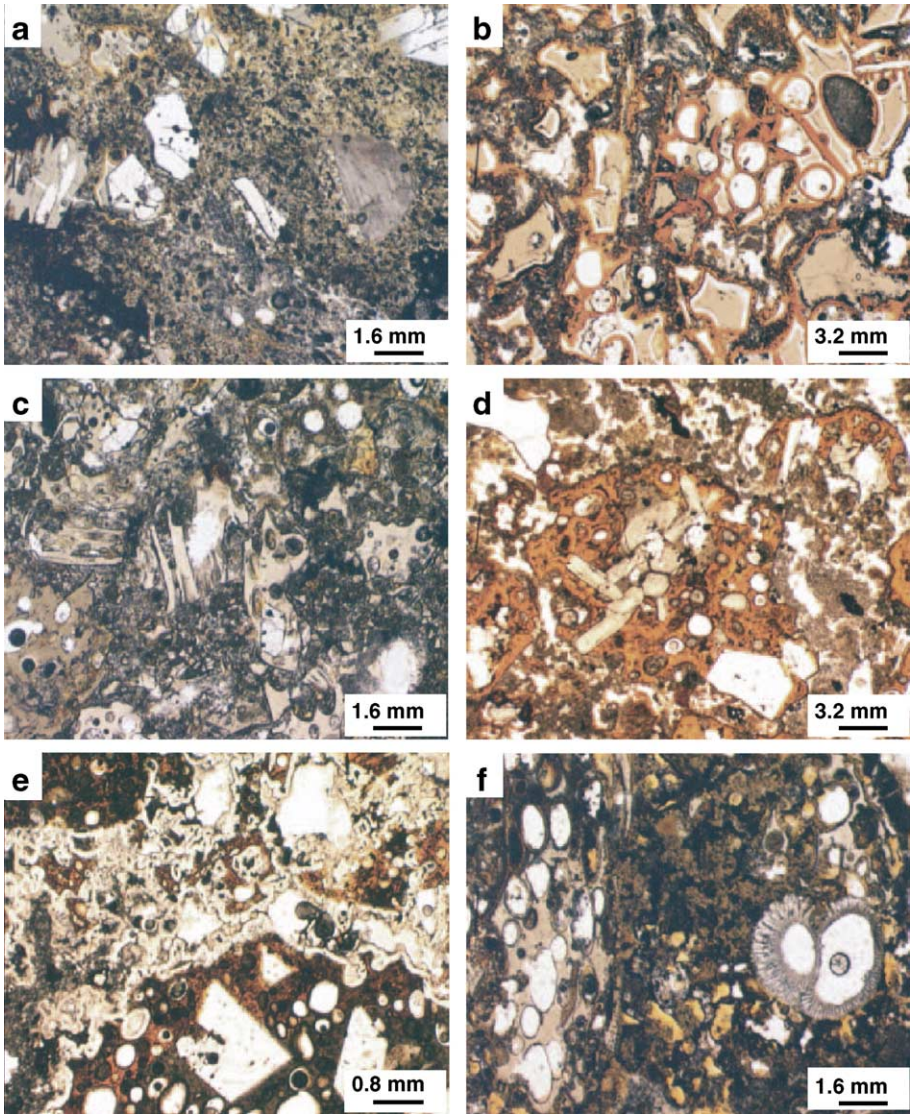

Fig. 6. Photomicrographs of samples from dives T272, T273, and T298. Images are in plane light. (a) Vesicular glassy pyroclast (center left), euhedral olivine phenocrysts, and detrital coralgal grain (right center) in fine altered matrix, T272-R2; (b) glassy vesicular lapilli with palagonite rims, clear space between orange palagonite and tan glass is shrinkage as palagonite dessicated, T273-R4; (c) variety of glass sand morphologies in T298-R3 ranging from elongate stretched vesicular grains to grains with round vesicles; (d) palagonitized lapillus with small fresh glass core remaining around cluster of titanaugite phenocrysts in T298-R12; (e) zeolite cement surrounding glass lapillus with fresh glass core in T298-R17; (f) vesicular glass lapillus with slightly elongate vesicles (center left), orange–brown palagonitized glass grains, and planktonic foraminifer (right center).

4.4. Whole-rock chemistry

Five lava samples were analyzed from the two cones on the Koko Rift (Table 2). The deeper, more westerly cone is composed of primitive alkalic basalt (T273-R1, -R5, and -R6) with 11.25 to 11.98 wt.% MgO. The primitive mantle normalized trace element data (Fig. 8) and the major element data are compositionally identical within analytical precision. These samples have small negative Y, Zr, Hf, and Pb anomalies; large negative U, Th, Rb, and Cs anomalies; a small positive Ti anomaly; and large positive P and Sr anomalies. These are the only samples from the Honolulu Volcanics or North Arch volcanic field that do not have strong negative K anomalies.

The 2 samples from the shallower eastern cone are primitive basanite (MgO = 12.66 and 12.74 wt.%) that contained secondary carbonate in vesicles. We treated these samples with a warm acetic acid wash prior to crushing the sample to remove the carbonate. The trace element data for the two samples are identical (Fig. 8) and are characterized by large negative Ti, Zr, Hf, K, U,

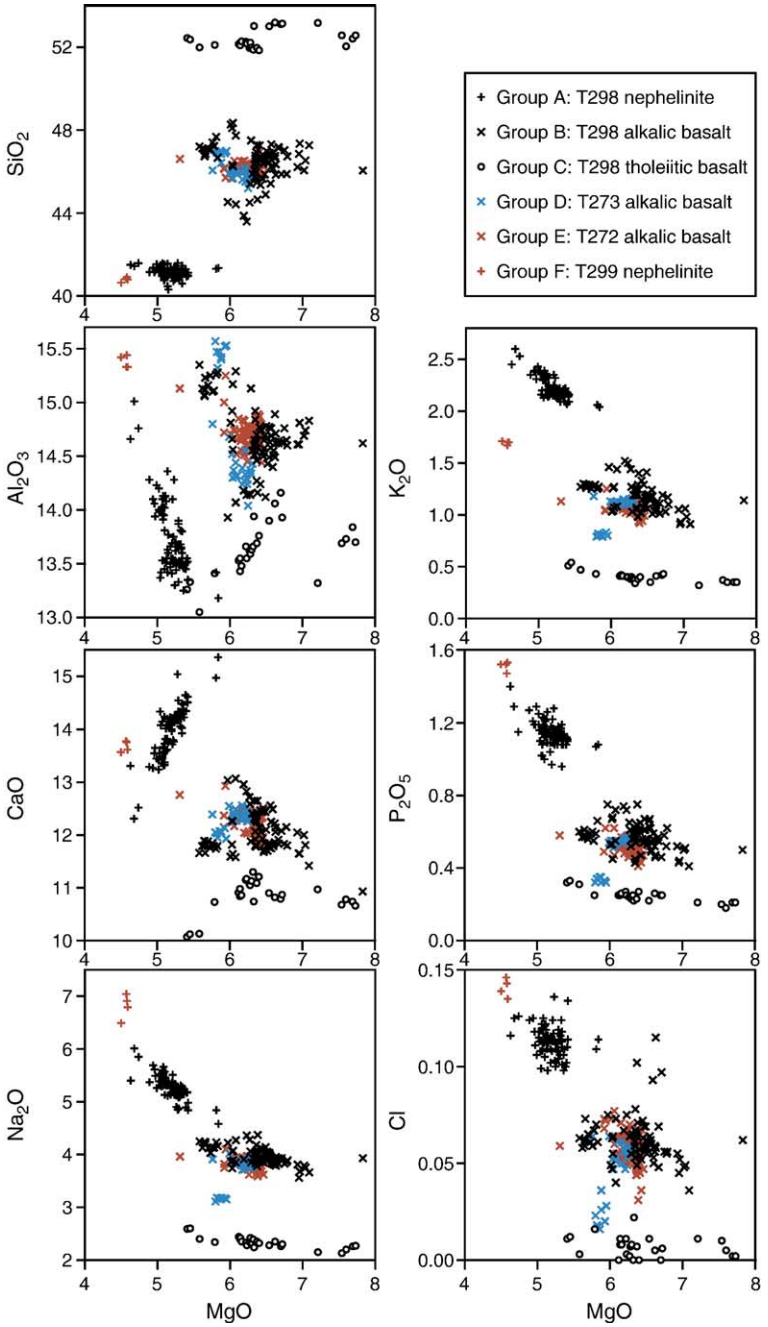

Fig. 7. MgO-variation diagrams of glass recovered during the four ROV dives. The groups are described in the text, as are the observed variations in composition. Plotted points include average compositions of glasses in volcaniclastic rock samples and individual point analyses of grains recovered in sediments.

Th, Rb, and Cs anomalies; a small negative Y anomaly; and large positive P and Sr anomalies.

4.5. Ar–Ar age data

The age spectrum for sample T273-R5 (Fig. 9c) is reasonably flat, with precision of individual steps on the order of ± 0.07 Ma, and radiogenic yields ranging from about 1% to 5%, and maximum K/Ca ratios on the order of 0.2. The weighted mean age of steps B to F is 0.14 ± 0.10 Ma, although the MSWD value for this interval is 4.0, attesting to some discordance greater than that attributable to analytical error. The data fail to form a well-defined linear array on an isotope correla-

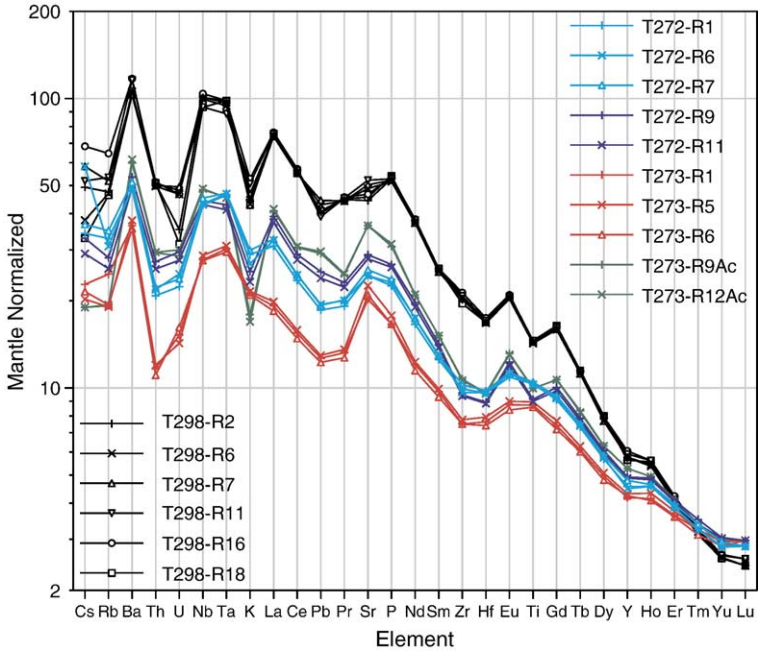

Fig. 8. Primitive-mantle-normalized (Sun and McDonough, 1989) logarithmic trace element plot. Five different sample groups from dives T298, T273, and T272 are shown in different colors. Key features of the patterns are the lack of negative K and Ti anomalies in Group D1 lavas, and the strong positive P and Sr anomalies and the strong negative Cs, Rb, U, Th, Zr, and Hf anomalies in all the lavas. These features are discussed in the text.

tion diagram and yield an isochron age younger that the weighed mean age of steps B to F.

The age spectrum of sample T273-R6 (Fig. 9d) is similar to that of T273-R5. Individual steps are slightly less precise (± 0.04 to ± 0.10) with radiogenic yields ranging from 0.4 to 2.6. K/Ca ratios are generally between 0.2 and 0.3. Although the entire age spectrum is somewhat less concordant that that of T273-R5, steps B to E are concordant, with an MSWD value of 0.66 and a weighted mean age of 0.14 ± 0.06 Ma. On an isotope correlation diagram, the data form a crude linear array with a near atmospheric $^{40}Ar/^{36}Ar$ intercept and an intercept age (0.10 ± 0.03 Ma) that overlaps with the weighted-mean age.

The age spectrum for sample T273-R9 (Fig. 9e) is relatively flat, although it appears slightly less reliable than the age spectra of the other two T273 samples. Step C is relatively precise (0.113 ± 0.023 Ma, radiogenic yield of 6.2%), but subsequent steps have lower radiogenic yields (-1.5% to 1.0%), poorer precision (± 0.04 to ± 0.05 Ma), and are somewhat discordant relative to step B, with steps C and D having negative to near zero ages. The weighted mean age of steps B to H is 0.06 ± 0.05 Ma. K/Ca ratios for this interval are on the order of 0.3. When plotted on an isotope correlation diagram, the data fail to form a well-defined linear array.

5. South flank of Diamond Head

5.1. Morphology and dive observations

Dive T272 was located on the south flank of Diamond Head (Fig. 10) in a region of hummocky, high-backscatter terrain. The dive started at 562 m depth and traversed north up a low, rough high-backscatter hill, through a saddle roughly 20 m deep with moderate backscatter, and then upslope through more high-backscatter rough terrain, finally ending at 494 m depth.

Much of the dive traversed similar terrain with sculpted volcaniclastic deposits draped over in-place pillow lavas (Fig. 11d). Irregular or patchy outcrops of volcaniclastic deposits occur interspersed between pillow lavas. The entire surface is dusted by moderate amounts of unconsolidated sediment. As the dive progressed upslope, the relative coverage of volcaniclastite increased, as did the thickness of the deposits (Fig. 11e). At one point, the depth increased as we continued towards shore. This saddle is buried in thick, unconsolidated rippled sediment at least 20 cm thick (push core length). Continuing towards shore, we encountered pillow lava and talus of pillow fragments. One isolated block of carbonate (Fig. 11f), apparently a large loose block that slid down from

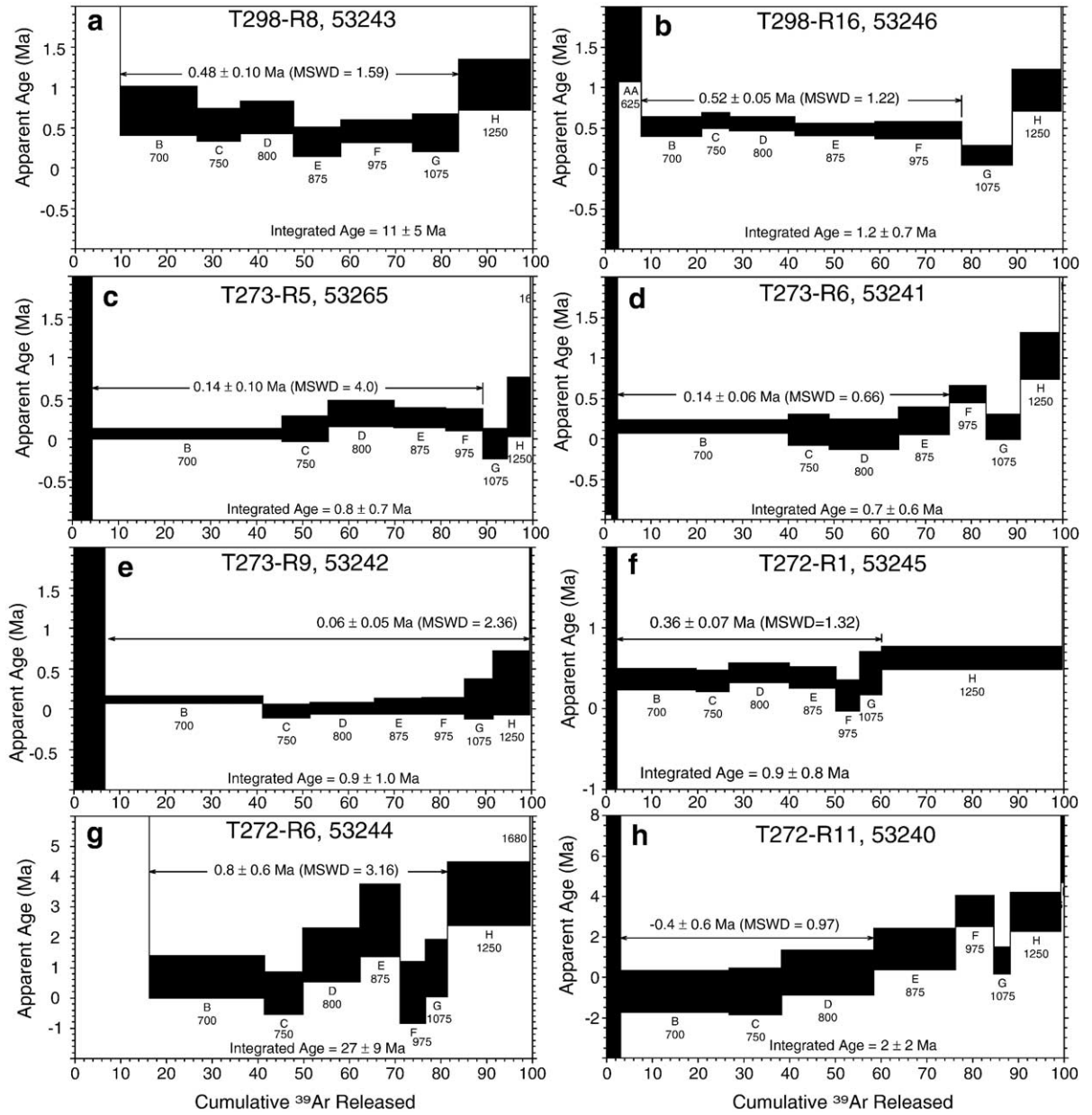

Fig. 9. Ar–Ar age spectra for samples T298-R8 (a) and T298-R16 (b) from the isolated cone off the northeast shore; T273-R5 (c), T273-R6 (d), and T273-R9 (e) from the submarine Koko Rift; and T272-R1 (f), T272-R6 (g), and T272-R11 (h) from the submarine slope of Diamond Head. Spectra and reliability of the argon age data are discussed in the text.

upslope, was encountered and sampled near the end of the dive.

5.2. Petrography

All the lava samples are dense to only slightly vesicular (<2%) and have similar mineralogy, containing only olivine microphenocrysts. Many of the samples have fine-grained quench groundmass textures, with samples R1, R6, and R11 having the most crystalline groundmass with the coarsest augite and plagioclase crystals. The volcaniclastic samples (R2, R3, and R4) are siltstones to sandstones with minor to abundant fresh glass shards remaining (Figs. 5a,b and 6a). Some glass shards have highly elongate bubbles (Fig. 5a and b). All three samples contain a minor component of carbonate coralgal grains (fragment center right in Fig. 6a). Sample R8 is a siltstone with

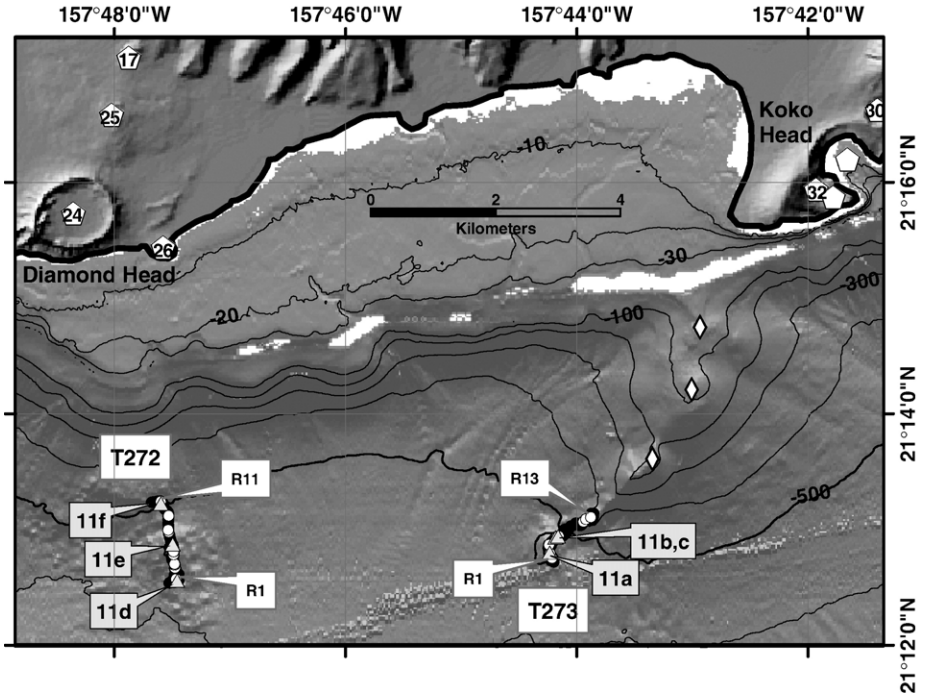

Fig. 10. Map showing the region on the south side of O'ahu and the dive tracks for *ROV Tiburon* dive T273 on the southwestern submarine extension of the Koko Rift and dive T272 on the southern flank of Diamond Head. The known subaerial vents of the Honolulu Volcanics are shown as pentagons labeled with vent group numbers from Jackson and Wright (1970). Previously unidentified vents along the Koko Rift are indicated by diamonds, with two additional westernmost vents beneath the dive track for T273. Offshore bathymetry as in Fig. 1 with additional nearshore Lidar data (U.S. Army Corps of Engineers, Mobile, Alabama; http://shoals.sam.usace.army.mil/default.htm). The locations of the bottom photographs in Fig. 11 are indicated along the dive tracks, as are the first and last rock sample collected during each dive.

about half volcanic and half fossiliferous carbonate grains.

5.3. Glass compositions

Analyses of 77 glass sand and lapilli from volcaniclastic sandstone and siltstone define a range of alkalic basalt compositions (Table 1; Fig. 2; Fig. 7, group E) with MgO ranging from 5.31 to 6.46 wt.%. Glass from volcaniclastite samples R2 to R4 are nearly identical and fall within the range of compositions of solitary glass sand grains extracted from PC63. None of the samples collected in the later, shallowest part of the dive had any unaltered glass. The analyses have some broad trends with lower MgO grains having higher Al_2O_3, CaO, Na_2O, K_2O, and TiO_2. The lower SiO_2 grains also have higher S (Fig. 12). A single analyzed glass inclusion in an olivine crystal contains about 0.2 wt.% S.

5.4. Whole-rock chemistry

The five analyzed samples from the south flank of Diamond Head are all primitive alkalic basalt (MgO = 11.63 to 12.33 wt.%) that can be divided into two slightly different compositional groups. The first group, the samples from deeper on the slope (T272-R1, -R6, and -R7) is slightly less enriched in light-REE (Fig. 8) and has small negative Y and Pb anomalies; a small positive Ti anomaly; large negative Zr, Hf, K, U, Th, Rb, and Cs anomalies; and large positive P and Sr anomalies. The second group of samples (T272-R9 and -R11) has a small negative Y anomaly; large negative Ti, Hf, Zr, K, U, Th, Rb, and Cs anomalies; and large positive P and Sr anomalies. This group has more light-REE enriched patterns and larger negative K and Ti anomalies compared to the first group.

5.5. Ar–Ar age data

Following low-precision initial steps, the age spectrum of sample T272-R1 (Fig. 9f) is reasonably flat near 400 ka, with a somewhat older final step near 600 ka. Uncertainties on individual steps are on the order of ± 0.06 Ma (uncertainties on individual steps are quoted at $\pm 1\sigma$). Radiogenic yields (the percent of ^{40}Ar that is radiogenic, as opposed to atmospheric)

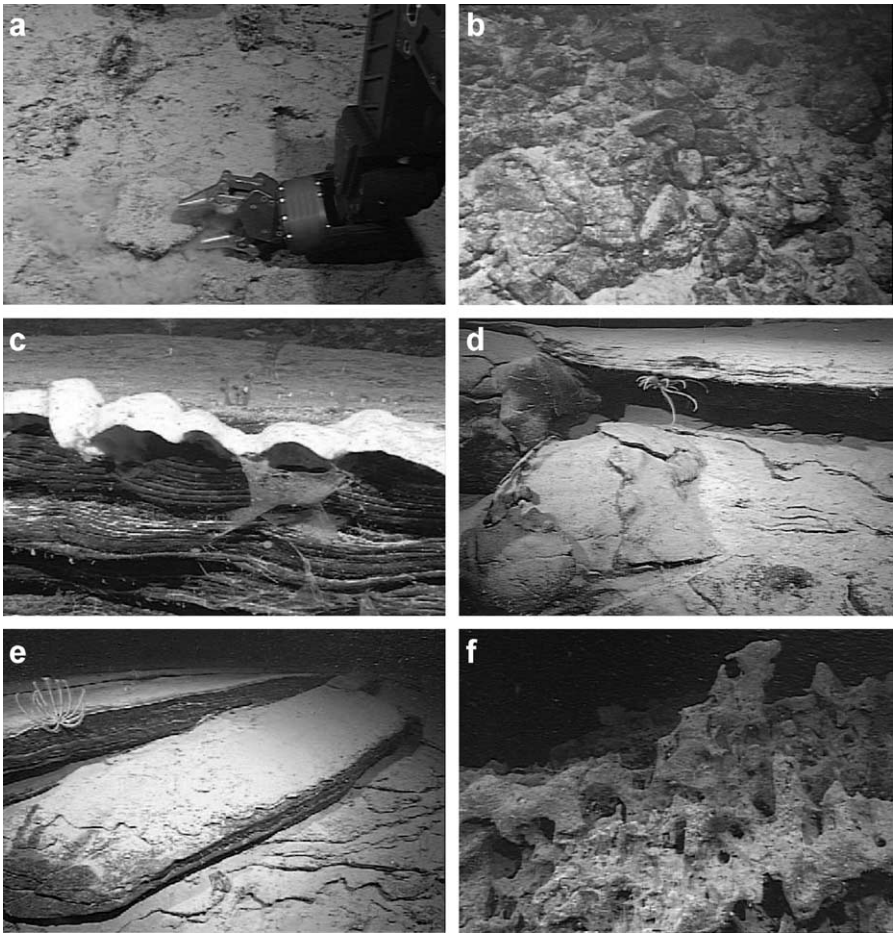

Fig. 11. Framegrabs of video recorded during *ROV Tiburon* dives T273 (a–c) and T272 (d–f). Each image shows an area of the seafloor roughly 3–4 m across. (a) Thin-bedded volcaniclastite deposits containing some angular clasts at 491 m; (b) pillow lava near collection site of T273-R6 and -R7 at 498 m; (c) cross-bedded fine volcanic ash beds near collection site of T273-R8 at 513 m; (d) thin-bedded volcaniclastite deposits draped over pillow lavas at 558 m; (e) thick-bedded volcaniclastite deposits at 513 m; (f) karstic carbonate block at 503 m.

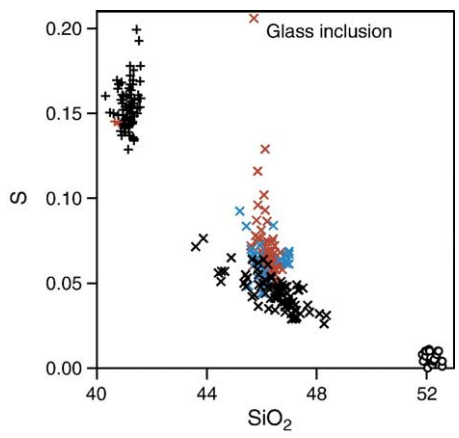

Fig. 12. S versus SiO_2 diagram for glasses. Symbols as in Fig. 6. A single glass inclusion in an olivine phenocryst in Group E glass is labeled.

vary from 0 to 5.8% throughout the bulk of the spectrum (excluding the final low-precision heating step). The K/Ca ratio (calculated from the measured ratio of $^{37}Ar_{Ca}/^{39}Ar_K$) is typical for a basalt, reaching a maximum near 0.6 in the low- to middle-temperature parts of the spectrum as glass and plagioclase degas then dropping at higher temperatures as low-K, high-Ca pyroxene degasses. A weighted-mean age calculated for steps B to G for this sample is 0.36 ± 0.07 Ma (all errors for calculated and intercept ages are quoted at 2σ). The MSWD value for this interval of the age spectrum is 1.3, indicating that all of the age variation among steps can be accounted for by analytical error. Because of the low radiogenic yields of individual analytical steps, the isotope correlation plot of this data appears as a tight cluster of points near the *Y*-axis rather than forming a well correlated linear array.

Nonetheless, the isochron intercept age (0.32 ± 0.04 Ma) is within error of the weighted mean age, and the $^{40}Ar/^{36}Ar$ intercept (297.1 ± 2.4) is within error of the atmospheric value (295.5).

The age spectrum for sample T272-R6 (Fig. 9g) is considerably less precise and more disturbed than that of the previous sample. Uncertainties on individual steps are on the order of ± 0.5 Ma. Radiogenic yields in the middle part of the age spectrum reach a maximum of only 2.7%. K/Ca ratios reach a maximum of only 0.2. The weighted mean age of steps B to G is 0.8 ± 0.6 Ma, although the high MSWD of 3.1 for this interval demonstrates that the age variation among steps is larger than can be accounted for by analytical error alone. The data do not define a sensible linear array on an isochron correlation diagram; the slope of the intercept age is positive, yielding a negative intercept age.

The age spectrum for sample T272-R11 (Fig. 9h) is even more problematic than T272-R6. Precision of individual steps is on the order of ± 0.6 Ma, and radiogenic yields for the majority of the age spectrum are close to zero. The age spectrum is strongly discordant, with ages of initial steps climbing from initial negative ages (reflecting uncertainties in correcting for large amounts of atmospheric ^{40}Ar) to more than 3 Ma. The mean age of the three relatively concordant lower temperature steps is -0.4 ± 0.6 Ma. The data fail to form a well-correlated array on an isochron correlation diagram.

6. Slope and canyon deposits

6.1. Locations and dive observations

Volcaniclastic deposits were observed on the northeast flank of O‘ahu during dive T298, both north and southwest of the isolated cone, and in a submarine canyon on the northeast flank of O‘ahu that was explored during dive T299 (Fig. 3).

After crossing over the solitary cone during dive T298, we continued through a trough consisting of bedded volcaniclastic deposits, sculpted by erosion (R19, PC78 and PC65; Fig. 4e). This region has moderate backscatter and extends about 0.75 km from the base of the cone. Farther south and moving upslope, the dive ended in rippled unconsolidated sediment (PC66 and PC69; Fig. 4f) that has low backscatter on the sonar maps. Some of the volcaniclastic deposits on the downslope side of the cone (R3 and R5) contain admixed slope deposits with distinct alkalic basalt glass compositions discussed below.

Dive T299 began in layered sediments exposed near the axis of the canyon and recovered several clasts transported down the canyon. This dive is included here only because a single volcaniclastic sample with fresh glass was recovered.

6.2. Petrography of recovered samples

The fine-grained pale glass that comprises much of the matrix in T298-R3, and occurs rarely in T298-R5, consists of highly vesicular fragments. Fluidal fragments are common (Fig. 13a, c, and f). Stretched-bubble scoria-like fragments (Fig. 13d and f) or thin bubble-wall fragments (Fig. 13a, b, and e) occur less frequently. In many fragments, bubbles are elongate (Fig. 13b, d, and f), coalesced (Fig. 13d, and f), or burst (Fig. 13c). Sample T298-R19 is volcaniclastic sandstone to lapillistone that is lithologically similar to the fine matrix grains in R3 and R5. It contains only olivine microphenocrysts and the lapilli-sized glassy clasts of alkalic basalt composition are highly vesicular (>50%, Fig. 6f) and are largely altered to yellow–brown palagonite. Some fragments are tachylite, but no crystalline rock fragments occur in the sample. Mixed in the volcaniclastite samples are rare planktonic foraminifers (Figs. 5f and 6f). Some clasts are highly fluidal (Fig. 5d) or highly vesicular (>90%, Fig. 5e). Loosely cemented volcaniclastite recovered in PC 65 is nearly identical in texture, composition, and alteration to R19. PC78, collected near R19, contains some of the volcaniclastic sands seen in R19 but is mainly unconsolidated biogenic sediment observed at the surface near the end of the dive. The silt-to-sand component of this composite sample contains planktonic and benthic foraminifera, sponge spicules, gastropod and bivalve shells and fragments, pteropods, rare squid beaks, abundant transparent green euhedral olivine crystals and glomerocrysts, and rare vesicular and dense glass fragments of alkalic and tholeiitic basalt composition, respectively (see glass chemistry section below).

Samples T298-PC66 and T298-PC69, collected at the end of the dive, are similar hemipelagic muds. The small silt-to-sand component consists of planktonic and benthic foraminifera, sponge spicules, pteropods, rare ostracods, radiolarians, gastropod and bivalve shells, wood and/or charcoal fragments, rare squid beaks, rare angular dense glass fragments of tholeiitic composition (see below), and rare, irregular, translucent yellow–green olivine crystals.

The samples from dive T299 all appear to be clasts transported down the canyon. One sample is a dense,

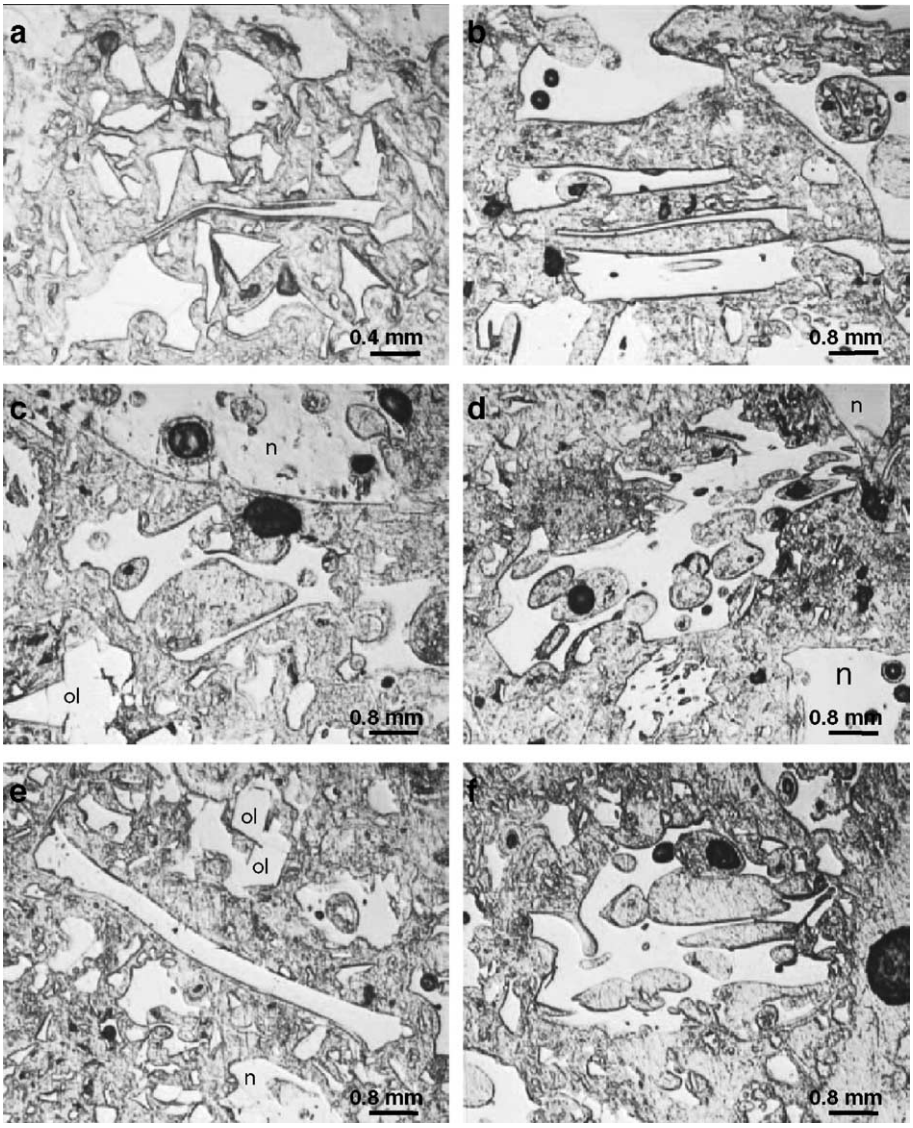

Fig. 13. Photomicrographs of glass pyroclasts in T298-R3, all in reflected light. (a) Fluidal hairpin-shaped pyroclast (center); (b) slightly curved limu o Pele fragment (center) and range of vesicular pyroclasts, some with elongate and others with round vesicles; (c) fluidal vesicular pyroclast with large burst vesicle; (d) lapillus with coalesced vesicles; (e) thick limu o Pele fragment; (f) fluidal vesicular lapillus with coalesced vesicles.

altered tholeiitic basalt (based on petrography) and three others are carbonate sandstones that include shallow water coralgal fragments, large foraminifers, other unidentified carbonate fragments, rare plagioclase and olivine crystals, and rare altered volcanic fragments. The final sample (R3) is another sandstone, but with about half carbonate sand grains and half vesicular, altered volcanic grains. A single lapillus has a fresh glass core remaining.

None of the samples was analyzed for whole-rock chemistry, isotopes, or Ar–Ar age dating due to their tiny size (individual sand and silt grains) or alteration characteristics.

6.3. Compositions of glass

From dive T298, we analyzed 78 glass grains from R19, from loosely cemented volcaniclastic deposits sampled by PC65 and PC78 upslope from the cone, and sand grains in R3 and R5 on the downslope side of the cone. These glasses are alkalic basalt (Fig. 7, group B) with a wide range of compositions (SiO_2=43.6–48.35 wt.%, MgO=5.58–7.83 wt.%, K_2O=0.91–1.52 wt.%, and S=260–760 ppm). There are two broad trends in the data with decreasing MgO: one to slightly higher SiO_2, higher Al_2O_3, and similar CaO, and the second to lower Al_2O_3 and SiO_2, and

higher CaO. Trends for other major elements are not well defined. The lower SiO_2 samples also have lower S contents than the higher-SiO_2 ones (Fig. 12). Several grains with the highest SiO_2 (around 48 wt.%) are more SiO_2-rich than any previously analyzed lava from the Honolulu Volcanics (Clague and Frey, 1982).

Glass analyses of 26 grains recovered from unconsolidated biogenic sediments (PC66, PC69, some in PC78) even farther upslope near the end of the dive are tholeiitic basalt with SiO_2 = 52.0–53.2 wt.%, MgO = 5.4–7.7 wt.%, K_2O = 0.32–0.54 wt.%, TiO_2 = 1.88–2.93 wt.%, and < 110 ppm S (Table 1; Fig. 7, group C). TiO_2, FeO, Na_2O, K_2O, and P_2O_5 increase with decreasing MgO, whereas Al_2O_3 and CaO first increase and then decrease at MgO below about 6.5 wt.%.

A single unaltered lapillus in R3 recovered during dive T299 is sodic nephelinite (Table 1; Fig. 7, group F) with up to 7.0% Na_2O. The four analyses plotted in Fig. 7 are from a single lapillus. Previously reported analyses of 13 nephelinite whole-rock lava samples from the Honolulu Volcanics have Na_2O between 2.6 and 4.5 wt.% (Clague and Frey, 1982), significantly lower than either the T299 or the T298 nephelinites reported here. For the most part, the compositions extend the trends of nephelinite compositions from dive T298 to lower MgO and higher Al_2O_3, Na_2O, P_2O_5, and Cl contents. However, the glass is higher in CaO and lower in TiO_2 and K_2O than extrapolation of the T298 trends would predict. Sen et al. (1996) presented analyses of interstitial melts in xenoliths with similar high alkalis, but much higher Al_2O_3, and we have analyzed a glassy rind on xenolith 88SAL1-4 from Salt Lake Crater with similar characteristics (cited in Sen et al., 1996). Similar high-Na_2O nephelinite glasses are reported from the slope of Kilauea Volcano (Sisson et al., 2002).

7. Radiogenic isotopic analyses

The subaerial Honolulu Volcanics have depleted, and generally moderately homogeous isotopic ratios with 14 samples having $^{87}Sr/^{86}Sr$ ranging from 0.70328 to 0.70348 and $^{143}Nd/^{144}Nd$ ranging from 0.51303 to 0.51308 (Stille et al., 1983; Roden et al., 1984; corrected to common standard values). Pb isotopic data are even more homogenous with 12 samples having $^{206}Pb/^{204}Pb$ ranging from 18.04 to 18.20, $^{207}Pb/^{204}Pb$ from 15.44 to 15.47, and $^{208}Pb/^{204}Pb$ from 37.69 to 37.83 (Sun, 1980; Stille et al., 1983). Only the samples reported by Stille et al. (1983) were analyzed for all three isotopic systems.

The submarine samples of the Honolulu Volcanics are also homogeneous, but have $^{87}Sr/^{86}Sr$ ratios at the high end of the range for subaerial Honolulu Volcanics (Table 3 and Fig. 14; Stille et al., 1983; Roden et al., 1984). Five of the samples have Nd isotopic ratios similar to previously reported values and one sample from the northeast cone has lower $^{143}Nd/^{144}Nd$ than previous reported for subaerial Honolulu Volcanics (Stille et al., 1983; Roden et al., 1984). Pb ratios slightly expand the range reported for subaerial Honolulu Volcanics lavas (Sun, 1980; Stille et al., 1983) with one Diamond Head sample having $^{206}Pb/^{204}Pb$ and $^{208}Pb/^{204}Pb$ higher than previously reported and samples from each dive having Pb ratios lower than the ranges cited above. Other than slightly expanding the ranges of values for the Honolulu Volcanics, the data for the submarine samples are similar to published data for subaerial samples. The nephelinite samples from the northeast cone (dive T298) required a more rigorous acid leaching for Sr isotopic

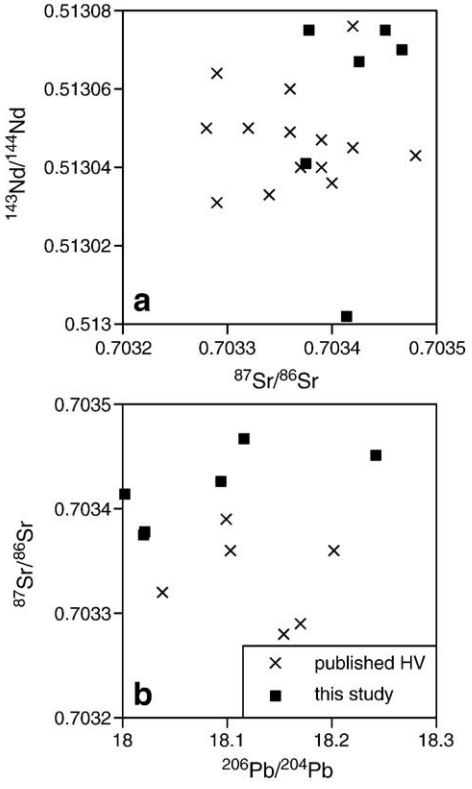

Fig. 14. Isotopic data for published subaerial Honolulu Volcanics samples (Stille et al., 1983; Roden et al., 1984) and for 6 samples from the submarine Honolulu Volcanics vents (Table 3). (a) $^{143}Nd/^{144}Nd$ versus $^{87}Sr/^{86}Sr$ and (b) $^{87}Sr/^{86}Sr$ versus $^{206}Pb/^{204}Pb$. The submarine lavas generally have slightly more radiogenic Sr isotopic ratios, but similar ranges of Nd and Pb isotopic ratios, compared to the subaerial lavas.

analyses. Our initial treatment, outlined in Table 3, was inadequate and led to anomalously radiogenic results.

8. Discussion

8.1. Distribution of Honolulu Volcanics vents

The swath bathymetry offshore Koʻolau Volcano (Fig. 1) increases the number of Honolulu vents from the 37 onshore and nearshore vents that formed small islands (Winchell, 1947) to 42 vents. Jackson and Wright (1970) defined a series of roughly parallel northeast-trending fissures along which most vents could be grouped. The offshore vents do not change their general interpretation. However, the new offshore data demonstrate how few additional vents occur on the submarine flanks of the volcano in comparison to the numerous vents on or close to the island. Even more striking is that 5 of the 6 submarine vents occur aligned with and adjacent to the 13 known vents comprising the Koko Rift. The data demonstrates that the Honolulu Volcanics erupted almost entirely through the island with the most distal vent only 12 km from the northeast shoreline.

Several of the lithologies recovered during dives T298 and T299 cannot be traced back to known vents. For example, all of the vents upslope in the vicinity of Ulupaʻu Head (labeled 1–6 in Fig. 2) are nephelinite or melilitite, so there is no known vent on the northeast side of Koʻolau that could be the source for these deposits. The recovered glasses range from submarine-erupted high-S (up to 760 ppm), lower-SiO_2 alkalic basalt compositions to low-S (as little as 260 ppm) higher-SiO_2 alkalic basalt compositions (see Fig. 12). Reiners and Nelson (1998) have documented changes in composition during rejuvenated-stage eruptions of the Kōloa Volcanics on Kauaʻi that progress from more to less alkalic. If decreasing S content in these glasses is interpreted to indicate decreasing eruption depth as the vent grew towards sea level, then the compositional sequence of this unknown Honolulu Volcanics vent is, like the Kōloa vents, from more to less alkalic. The low S contents of the least alkalic glasses suggest that the vent approached, but did not breach, sea level. The vent may be located northeast of Ulupaʻu Head, buried beneath younger reef deposits that form several terraces shallower than 100 m deep (Fig. 3). The most likely location is near 157°41′30″, 21°28′40″ where a northeast oriented flat-topped ridge rises above 100 m depth.

Likewise, the sodic nephelinite composition of the glass recovered during dive T299 is unknown from any vent in the Honolulu Volcanics. The high-S in this glass suggests that it erupted below sea level from a vent now buried beneath later-formed vents in the vicinity of Ulupaʻu Head.

Dive T272 on the flank of Diamond Head recovered lavas having two distinct compositions with the shallower samples (R9 and R11) being less alkalic and therefore larger degree melts than the deeper samples (R1, R6, and R7). Since there is a small saddle between these samples, it is possible that the deeper samples were erupted from a separate small vent on the flank of Diamond Head. However, the sequence here is also consistent with evolution from earlier (downslope) smaller-melting-degree more-alkalic magmas to less-alkalic larger-melting-degree magmas with time, as proposed by Reiners and Nelson (1998) for vents of the Kōloa Volcanics on Kauaʻi. Although no intermediate composition glasses or rocks were recovered, we prefer this interpretation as a hypothetical vent on the flank of Diamond Head would be of miniscule volume.

8.2. Eruption styles

The submarine vents each consist of lava flows and volcaniclastic deposits that range from fine-bedded ash to volcanic breccia. The young age of the vents and the relative vertical stability of Oʻahu (Moore, 1987) indicate that the vents are situated at approximately the same depth at which they formed. The summit of the isolated cone on the northeast flank of the island, at about 590 m depth, consists of breccia and lapillistone consisting of vesicular glassy clasts. The lack of finer-grained deposits suggests that these volcaniclastic deposits formed during pyroclastic eruptions, with little role for seawater beyond quenching the ejected magma clots to glass. The glass contains high concentrations of S (average 1500 ppm), consistent with their nephelinite composition and submarine eruption (Dixon et al., 1997). The coarse clast sizes and confinement of deposits to the flanks of the cone suggests that activity was not highly energetic; such eruptions were probably strombolian. Lava fragmentation was apparently caused by exsolution and escape of large amounts of magmatic volatiles, as has been proposed for as deep as 4200 m around Hawaiʻi for similar strongly alkalic magmas (Davis and Clague, 2005) or as deep as 3800 m along the Gorda Ridge for mid-ocean ridge basalt compositions (Clague et al., 2003). The summit of the cone consists of blocky lava flows that resemble talus deposits, except they occur at the summit of the cone. These lavas erupted effusively and formed blocky flows. Such flow forms suggest the lava was more viscous than that

producing pillow lava, consistent with their fractionated compositions (5–5.4 wt.% MgO) and vesicle- and crystal-rich petrography. The alkalic basalt fragments in the deposits that blanket the slope on the northwest side are highly vesicular (Fig. 13) and retain significant volatiles in the quenched glasses (Fig. 12), consistent with formation during submarine pyroclastic eruptions. The deposits consist only of fine-grained fragments, suggesting that the fragments were transported down slope from a shallower eruption site.

Other deposits on two vents on the submarine extension of the Koko Rift, at depths of 450 and 370 m, are dominantly fine-bedded ash. These deposits are most likely ash produced during Surtseyan eruptions that occurred at the depth of the top of the cones or slightly deeper (<500 m). The ash was apparently erupted from the cones and was deposited by density currents on their slopes. The glasses have intermediate S contents (440–920 ppm) consistent with their submarine eruption. These same cones also have blocky lava flows whose flow forms are again consistent with viscous lavas with fractionated glass compositions (6–6.4 wt.% MgO) that are crystal-rich.

Dense pillows with small pillow buds on the flank of Diamond Head are draped by younger bedded ash deposits. Fresh undegassed glasses in fine-grained volcaniclastite samples have S contents ranging from 440 to 1290 ppm, consistent with submarine eruption. A single glass inclusion in an olivine contains 2060 ppm S, suggesting that the melt contained at least this much S prior to degassing at shallow depths, during which 37–79% of the initial S was lost. The S data are consistent with formation of the ash deposits during submarine Surtseyan eruptions as Diamond Head grew upwards towards sea level. Underlying pillow lavas are dense, most likely distal, flows of submarine erupted effusive lavas that predate the Surtseyan eruptions that formed Diamond Head. No degassed glass was recovered so either glasses formed during the subaerial phase of Diamond Head's growth were not transported down slope as far as the dive location or the quenched fragments are completely altered to palagonite.

8.3. Petrogenesis of lavas

8.3.1. Tholeiitic glass from dive T298

The compositions of the tholeiitic glass grains recovered during dive T298 do not match the high-SiO_2 character of late Ko'olau lavas erupted during the Makapu'u stage (e.g. Frey et al., 1994; Hauri et al., 1996; Jackson et al., 1999) but are similar to the lower-SiO_2 (Mauna Loa-like) lavas recovered from deeper in the shield by the Ko'olau Scientific Drilling Project (Haskins and Garcia, 2004) and to numerous samples recovered from the offshore blocks of the Nuuanu landslide which were derived from Ko'olau Volcano (Tanaka and Nakamura, 2002; Shinozaki et al., 2002; Clague et al., 2002). We infer that the tholeiitic glasses recovered from the northeast flank of Ko'olau erupted, probably from within Ko'olau caldera based on their location, before the transition to high-SiO_2 Makapu'u stage lavas slightly after 2.9 Ma (Haskins and Garcia, 2004). The lack of younger Makapu'u stage glasses suggests that such lavas did not overflow the caldera bounding faults on the northwest side of the caldera.

The tholeiitic glasses are all evolved melts derived from a narrow range of parental melts by crystal fractionation. Both olivine and then multiphase crystallization stages are represented by the melt compositions. All elements increase as MgO decreases down to about 6.8 wt.% during olivine crystallization. Al_2O_3 and then CaO decrease while all other elements increase as MgO continues to decrease as plagioclase, augite, and pigeonite crystallize, similar to other tholeiitic lavas in Hawai'i (Helz, 1987; Clague et al., 1995). Al_2O_3 begins to decrease at about 6.8% MgO but CaO does not peak until about 6.3 wt.% MgO, suggesting that plagioclase crystallization begins at about 1168 °C and is followed by augite crystallization at about 1157 °C, applying the geothermometer for compositionally similar Mauna Loa glasses (Montierth et al., 1995). The temperature at which plagioclase first appears is similar, but augite crystallization is suppressed (compared with melts; Helz and Thornber, 1987) by about 10 °C, presumably due to the lower CaO content of Mauna Loa and these Ko'olau melts compared with Kīlauea melts.

The low S contents indicate that these glass grains were derived from subaerially erupted and degassed lavas during the shield stage of Ko'olau Volcano, presumably from numerous flows that entered the ocean where explosive secondary (littoral) eruptions produced the glass grains. The grains formed at the coast were then transported downslope, mixed with biogenic sediment on the slope, and deposited where we collected them.

8.3.2. Submarine Honolulu Volcanics lavas

All the rocks are alkalic, ranging from alkalic basalt (all T272 samples, T273-R1, -R5, and -R6), through basanite (T273-R9, and -R12), to nephelinite (all T298 samples, T299-R3. Glasses from each location are distinctive but the compositions, with the exception of a sodic nephelinite glass from dive T299, are broadly similar to whole-rock compositions previously found

for the subaerial Honolulu Volcanics (Clague and Frey, 1982).

The trace element characteristics of rejuvenated stage lavas from O'ahu, Kaua'i, and the North Arch (Clague and Frey, 1982; Feigenson, 1984; Clague and Dalrymple, 1988; Clague et al., 1990; Maaloe et al., 1992; Dixon et al., 1997; Frey et al., 2000; Yang et al., 2003) are consistent with partial melting of a garnet lherzolite source, leaving varying amounts of residual garnet, clinopyroxene, and olivine, and at low degrees of melting, phlogopite and Fe–Ti oxides. New glass and whole-rock data on submarine samples allow us to evaluate: (1) the primitive or near-primary character of the magmas and melts in the Honolulu Volcanics; (2) the behavior during partial melting of some elements (such as Na, K, Rb, Sr, and Ba) that may be mobile during post-eruptive weathering of subaerial lavas (Clague and Frey, 1982); and (3) the spatial distribution of lava characteristics that reflect either variability in melting processes or source composition and mineralogy.

The off-shore Honolulu Volcanics whole-rock analyses have high MgO (11.25 to 12.90 wt.%), Ni (254–307 ppm), and Cr (414–539 ppm), consistent with primitive or near-primary magmas, as seen for nearly all the lavas on land. The major element analyses are shown on P_2O_5-variation diagrams in Fig. 15 with data for subaerial Honolulu Volcanics (Clague and Frey, 1982), Kōloa Volcanics on Kaua'i (Clague and Dalrymple, 1988) and for North Arch volcanic field samples (Clague et al., 1990). The submarine lavas generally plot within the fields for subaerial Honolulu lavas and have compositional trends similar to all three rejuvenated stage groups of lavas. Glass analyses from the subaerial Honolulu Volcanics have not been reported, reflecting the rarity of glass in the subaerial environment. Glass compositions of the submarine samples, however, are all evolved melts with low MgO contents (ranging from 4.56 to 7.83 wt.%) and demonstrate that these near-primary magmas consist of low-MgO, low-temperature, Kīlauea melts that contain abundant olivine and (sometimes) augite microphenocrysts. The submarine Honolulu magmas have therefore cooled significantly during transit through the upper mantle and crust, but the melt and crystals did not separate.

Similar observations have been made of the North Arch lavas (Clague et al., 1990) where 15 of 23 whole-rock analyses have MgO > 10 wt.% but the glasses have 35 of 36 compositional groups with MgO < 10 wt.% and 26 have MgO < 8 wt.%. Clague and Dixon (2000) argued that the more evolved melt compositions in the North Arch, compared to the near-primary magmas of the on-land rejuvenated stage lavas like the Honolulu Volcanics, reflected transport through cold lithosphere away from the islands compared to transport through lithosphere heated by the plume beneath the islands. Most of the glasses from the submarine Honolulu Volcanics are from clastic deposits and are highly vesicular. They therefore represent melt compositions erupted at the vents. The new data suggest that both the North Arch and Honolulu Volcanics are mostly near-primary magmas consisting of evolved melts that cooled and crystallized small olivine and, in some cases, augite microphenocrysts during melt migration, and that in each case the melt and crystals did not fractionate significantly during transport.

The submarine samples, even those treated with mild acid to remove secondary carbonate, appear to be little affected by post-eruptive element mobility of Na, K, Rb, Ba, and Sr (Fig. 8) compared with the variability observed for subaerial samples (Clague and Frey, 1982). We noted that Cs, Rb, U, K, Pb, and Sr varied among the six nephelinite samples from dive T298, and these variations suggest limited element mobility, particularly for Cs, in the more strongly alkalic lavas. Likewise, it appears that the more alkalic subaerial lavas have been the most susceptible to incompatible element mobility during late stage crystallization and alteration (Clague and Frey, 1982). These elements form linear trends with other highly incompatible elements such as La, unlike the broad scatter observed in their subaerial counterparts.

The new isotopic data indicate that the time-averaged composition of the source region for both on-shore and off-shore Honolulu Volcanics was depleted and homogeneous, with the possibility of a small increase in Sr-isotopic ratios for the offshore region (Fig. 14). The isotopic homogeneity of the samples allows us to use relatively simple melting models to evaluate melting processes and source mineralogy.

For example, models developed by Yang et al. (2003) suggest that the source of the North Arch lavas contained significantly more garnet and more clinopyroxene than the source for the subaerial Honolulu Volcanics. The steeper positive slope for the submarine Honolulu Volcanics samples on a Tb/Yb–Th plot (Fig. 16a) than for either the North Arch or the subaerial Honolulu Volcanics suggests that the source for the submarine Honolulu Volcanics lavas has even more garnet than the North Arch source. The source region for these rejuvenated stage lavas is strongly zoned with low garnet content beneath the island and greater garnet content peripheral to the island, then lower (but not as low as beneath the island) garnet

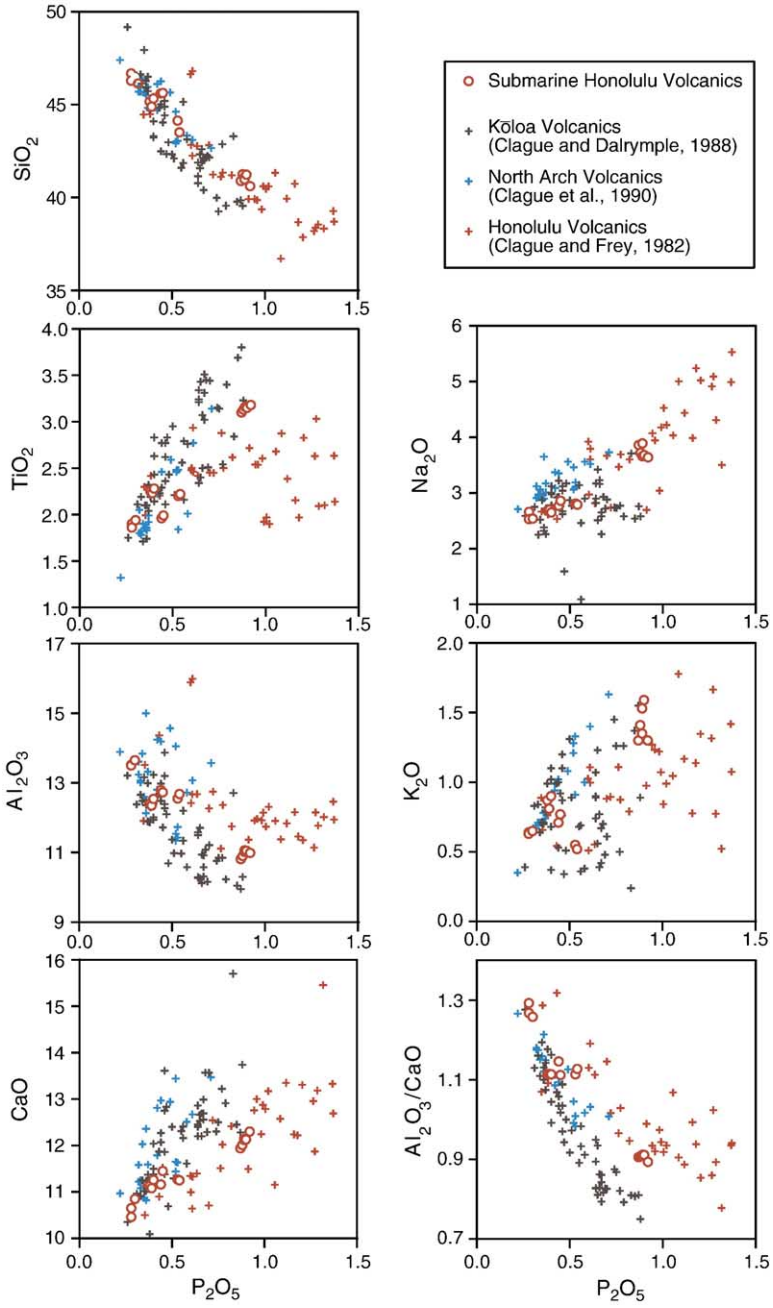

Fig. 15. P_2O_5-variation diagrams for whole-rock compositions from submarine vents of the Honolulu Volcanics and comparable data for rejuvenated stage lavas from the subaerial Honolulu Volcanics (Clague and Frey, 1982), subaerial Kōloa Volcanics on Kaua'i (Clague and Dalrymple, 1988) and from the submarine North Arch volcanic field (Clague et al., 1990). All the whole-rock data was normalized on a dry-reduced basis.

content several hundred kilometers from the island (beneath the flexural North Arch). The submarine Honolulu Volcanics have roughly constant Zr/Sm (Fig. 16b) and a positive slope on a Zr/Tb–Th plot (Fig. 16c) in contrast to the subaerial Honolulu Volcanics, which have the opposite (although the subaerial Honolulu samples are more scattered). These relations indicate that $D_{Sm} \sim D_{Zr} < D_{Tb}$ for the submarine Honolulu Volcanics compared to having $D_{Sm} < D_{Zr} \sim D_{Tb}$ for the subaerial Honolulu Volcanics. These differences are similar to the differences between group A and B lavas from the North Arch, which Yang et al. (2003)

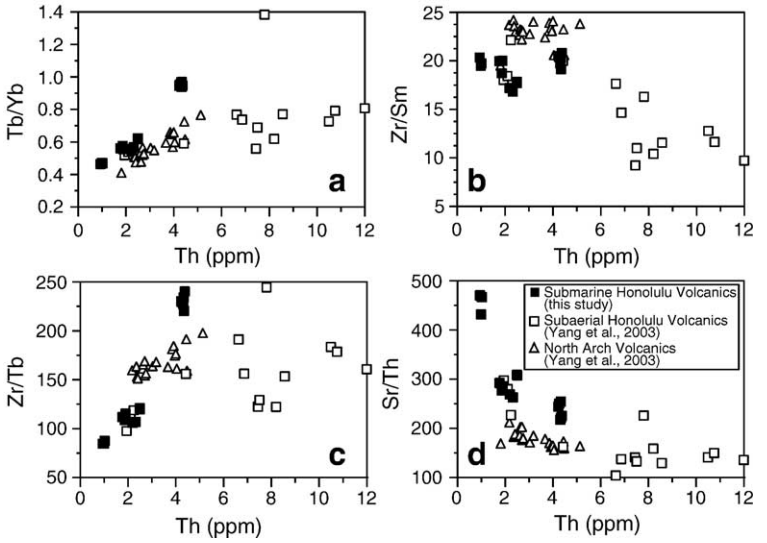

Fig. 16. a) Tb/Th versus Th for submarine and subaerial Honolulu Volcanics and for North Arch Volcanics. Data sources indicated on figure. b) Zr/Sm versus Th, symbols as in (a). c) Zr/Tb versus Th, symbols as in (a). d) Sr/Th versus Th, symbols as in (a). See text for discussion.

attributed to different proportions of garnet or Fe–Ti oxides in the sources, with a greater amount in the source for the offshore samples. This spatial zonation of source mineralogy occurs despite the nearly homogeneous isotopic composition of the sources.

Yang et al. (2003) also inferred that the source for the Honolulu Volcanics was characterized by K depletion and Ba enrichment. The submarine samples also have relative Ba enrichment, although the primitive mantle-normalized plots suggest that the apparent enrichment is due to depletions in adjacent Cs, Rb, U and Th. The depletion in Th relative to Ba results in high Ba/Th, a characteristic of Hawaiian lavas (e.g. Yang et al., 2003). Some of these samples have even higher Ba/Th (up to about 265) than previously reported for Hawaiian lavas. The lack of a negative K anomaly (Fig. 8) for the deep group of samples from the Koko Rift (T273-R1, -R5, -R6) suggests that the K depletion results from the melting process rather than from an inherent source characteristic. This observation suggests that the K depletion observed in all the subaerial Honolulu Volcanics, as well as the North Arch Volcanics probably results from K retention in phlogopite or amphibole during melting and that only during the largest degrees of melting is this residual K-rich phase completely exhausted.

The trace element data also show that Sr is enriched in these samples (Fig. 8), as previously noted for subaerial Honolulu Volcanics and North Arch Volcanics samples by Yang et al. (2003). The submarine samples with the greatest Sr enrichment have the lowest Th and are the largest degree partial melts (Fig. 16d). The isotopic analyses for several samples from T298 (Table 3) suggest that some portion of the Sr enrichment may be due to seawater addition since Sr isotopic ratios decrease with more severe acid leaching. However, simple mass balance calculations show that no more than about 40 ppm Sr with seawater Sr isotopic ratio could be added to these samples which contain in excess of 900 ppm Sr. Thus the effects of seawater addition are limited to 5% of the Sr present and do not account for the much larger Sr enrichments observed in most samples. A similar Sr enrichment in glass inclusions in olivine crystals in tholeiitic lavas from Mauna Loa Volcano has been attributed to a recycled ocean crust effect where the chemical signature of cumulus "ghost" plagioclase is preserved in eclogite in the source region (Sobolev et al., 2000). The Sr enrichment in the submarine Honolulu Volcanics samples could reflect the same ocean crust signature, although these samples also have a smaller enrichment in P, which has similar incompatibility to Sr. Simultaneous enrichment of Sr and P is unlikely to result from a "ghost" plagioclase effect of recycled ocean crust, but could result from incorporation of an altered crustal component.

8.4. Ages

We collected numerous pillow lava (Figs. 4a and 11b) and blocky lava (Fig. 4d) fragments, but none retained any glass rind. The young ages of the submarine Honolulu Volcanics vents, discussed below, appear at odds with this observed lack of glassy rinds on the lava flows observed and collected. This discrepancy is

so striking that at first we thought the lack of glass was an indication that the Honolulu eruptions were older than previously proposed. The rate of glass replacement by palagonite is, however, exponentially dependent on temperature (e.g. Moore et al., 1985) and the lack of glass rinds is consistent with alteration in warm, relatively shallow waters. Water temperatures, measured during the dives where these samples were collected, ranged from 4.5 °C at 870 m to 10.2 °C at 380 m, consistent with alteration rates up to 5 times more rapid (Moore et al., 1985) than in typical deep water environments where water temperatures are generally only a few degrees.

The age spectra from all eight samples (Fig. 9) begin with one or more highly imprecise steps, which, in some cases, are anomalously old. These initial steps reflect low-temperature release of large amounts of atmospheric argon, probably chiefly from hydrated matrix glass and interstitial authigenic clay. The anomalously old apparent ages of some of the initial steps in some cases are probably due to excess ^{40}Ar in the glassy matrix, although swamping of the mass spectrometer's electron multiplier detector by large atmospheric argon signals and remaining reactive gasses may also have affected the accuracy of measurement of these steps. Following these initial irregular, low-precision steps, the age spectra of all eight samples tended to become more precise and generally flatter, although the precision of individual steps and the degree of discordance vary widely from sample to sample.

^{40}Ar^{39}Ar dating results from these samples are considerably better than those obtained from many other young basalts erupted in submarine or littoral environments (for example, Duncan and Hogan, 1994). Complicating factors in dating such basalts include low K_2O contents, excess ^{40}Ar in glass (Dalrymple and Moore, 1968) and overwhelming amounts of atmospheric ^{40}Ar and reactive gasses released from hydrated glass and authigenic phases, especially clays. Efforts were made in this study to minimize these effects by electron microprobe characterization followed by ultrasonic and HCl acid treatments to reduce observed authigenic phases. Because of the young age and uniformly low radiogenic yields of the analyzed samples, weighted mean ages of flat central portions of the age spectra are preferred to isochron intercept ages determined from poorly defined arrays on isotope correlation diagrams. This approach is supported by the near atmospheric ^{40}Ar/^{36}Ar ratios of the low-temperature, low-radiogenic-yield steps which follow anomalously old initial steps, arguing against a homogeneous trapped component containing significant excess ^{40}Ar. However, there is still some uncertainty about the role of excess ^{40}Ar in these rocks. The old apparent ages of some of the initial heating steps (as old as 213 ± 30 Ma for the first heating step of T272-R6) may reflect mantle derived excess ^{40}Ar trapped in glass (Dalrymple and Moore, 1968), but these initial measurements were analytically compromised by huge atmospheric ^{40}Ar signals, as well as by large amounts of reactive gases which inhibited gas cleanup prior to measurement. It is unlikely that the weighted mean apparent ages are strongly affected by excess ^{40}Ar which would make them appear much older than their actual eruption ages. However, the possibility that small amounts of excess ^{40}Ar are having some effect on the quoted weighted mean ages cannot be entirely discounted. Some or all of the discordance observed in the age spectra may be due to reactor-induced recoil of ^{39}Ar from relatively high-K phases into relatively low-K phases. Recoil related discordance in age spectra is not uncommon in fine-grained polymineralic samples, particularly where fine-scale alteration has occurred (e.g. Lo and Onstott, 1989).

The highest quality results were obtained from samples T298-R8 and T298-R16. The weighted mean ages of these two samples, 0.48 ± 0.10 Ma and 0.52 ± 0.05 Ma, respectively, agree closely, and their weighted mean age, 0.51 ± 0.04 Ma, is considered the best estimate of their eruption age and the formation of the solitary cone northeast of O'ahu. Nearby cones on Ulupa'u Head have ages ranging from 0.4 to 0.7 Ma (Ozawa et al., 2005).

The age of the northeast cone relative to the age of the eruption that formed the alkalic basalt glasses recovered during dive T298 is not certain. Several volcaniclastic samples (R3 and R5) from the base of northwest base of the cone consist of nephelinite lapilli and alkalic basalt sand grains. All other volcaniclastic samples are either all nephelinite (R4, R10, R12, PC73, PC68) or all alkalic basalt (R19, PC65) fragments. The grainsize relations show that the alkalic basalt grains are distal turbidites compared to the local origin of the nephelinite lapilli, and the presence of alkalic basalt glass fragments in mixed lithology samples from the downslope side of the cone suggests that the cone postdates the emplacement of the alkalic basalt turbidites, and that the pyroclastic deposits from the cone entrained existing alkalic basalt sands.

Results from samples T273-R5, T273-R6, and T273-R9 from the submarine southwest end of the Koko Rift are of somewhat lower quality, reflecting their lower K_2O content and glassier, more altered matrix. Weighted mean ages from these three samples

are 0.14 ± 0.10 Ma and 0.14 ± 0.06 Ma for the deeper southwestern cone, and 0.06 ± 0.05 Ma for the northeastern cone. These weighted-mean ages overlap at 2σ and the weighted mean of all three is 0.10 ± 0.06 Ma. However, given the discordance and lower radiogenic yields of much of the age spectrum of T273-R9, the weighted mean of T273-R5 and T273-R6 of 0.14 ± 0.05 Ma, is our best estimate for the eruption age of the deeper cone. The shallower cone could be the same age or slightly younger. These age estimates are between those previously reported for vents along the subaerial Koko Rift by Gramlich et al. (1972) and Lanphere and Dalrymple (1980), but in general agreement with new ages between 0.06 and 0.10 Ma reported by Ozawa et al. (2005).

Samples T272-R1, T272-R6, and T272-R11 from the submarine flank of Diamond Head yielded the lowest quality results in this study, also reflecting their low K_2O and glass-rich, variably altered interstitial matrix. The age spectra of T272-R6 and T272-R11 are discordant and have low radiogenic yields. Their weighted mean apparent ages (0.81 ± 0.62 Ma and −0.43 ± 0.63 Ma respectively) have low precision and questionable accuracy, and are not considered reliable estimates of eruption age. The age spectrum of sample T272-R1 is more concordant and has higher radiogenic yields. The weighted mean age of T272-R1, 0.36 ± 0.07 Ma, may be an accurate estimate of the eruption age of Diamond Head. This age is consistent, within analytical precision, with reported ages of the overlying Black Point basalt (0.29 ± 0.01 Ma, Gramlich et al., 1972; 0.41 ± 0.04 Ma, Stearns and Dalrymple, 1978; and 0.369 ± 0.012 Ma, Ozawa et al., 2005) and an age of 0.38 ± 0.06 Ma for the overlying Kaimuku lava flow (Ozawa et al., 2005), and suggests that the Diamond Head tuff and the conformable Black Point basalt erupted closely in time and space.

9. Conclusions

(1) Lavas and volcaniclastic deposits were observed and collected from 4 submarine cones that are part of the Honolulu Volcanics on O‘ahu, Hawai‘i.

(2) The locations of these vents demonstrate that nearly all the vents of the Honolulu Volcanics are located on or very close to the shoreline of O‘ahu, with the most distal vent just 12 km offshore.

(3) The clastic samples and outcrops range from coarse breccias to cross-bedded ash deposits and show that explosive volcanism occurred at depths between about 350 and 590 m.

(4) The eruptive styles appear to be dominantly effusive to strombolian at greater depths, but apparently include violent phreatomagmatic explosive activity at the shallower sites along the submarine southwest extension of the Koko Rift.

(5) The compositions of the recovered samples are broadly similar to the strongly alkalic subaerial Honolulu Volcanics lavas, but the submarine lavas, erupted further from the Ko‘olau caldera have slightly more radiogenic Sr isotopic ratios, and trace element patterns that are distinct from either the subaerial Honolulu Volcanics or the submarine North Arch lavas.

(6) Trace element patterns are characterized by moderate to strong positive Sr and P anomalies, and moderate to strong negative Cs, Rb, U, Th, Zr, and Hf anomalies. Most samples have strong negative K and moderate Ti anomalies, as do all subaerial Honolulu Volcanics and North Arch samples, but one group of samples from the Koko Rift lack this chemical signature.

(7) The data are consistent with more garnet in the source region for the off-shore samples than for the on-shore Honolulu Volcanics lavas and indicate that the minerology of the source is zoned away from the islands, despite the homogeneous isotopic characteristics of the on-shore and off-shore samples.

(8) Ar–Ar ages show that eruptions at the submarine vents and Diamond Head occurred between about 0.5 Ma and 0.1 Ma, with the youngest ages from the Koko Rift, in general agreement with most published ages for the formation.

Acknowledgements

We thank Captain Ian Young and the crew of the *R/V Western Flyer* and Chief Pilot Dale Graves and the *ROV Tiburon* crew for their successful efforts to complete the dives under less-than-ideal weather conditions during the MBARI Hawai‘i expedition in Spring 2001. Without their dedication to getting the job done and done well, none of these dives would have been completed. We also thank the rest of the scientific party on the ship (Kristen Benchley, Rendy Keaten, Juli Morgan, Charlie Paull, Josh Plant, Kyra Schlining, Bill Ussler, and Jerry Winterer) who ably assisted in completing all the dives and describing and curating the many samples recovered.

References

Beeson, M.H., Jackson, E.D., 1971. Origin of the garnet pyroxenite xenoliths at Salt Lake Crater, Oahu. Spec. Pub., vol. 3. Mineral. Soc. Am., Madison, Wisconsin, pp. 95–112.

Clague, D.A., Dalrymple, G.B., 1988. Age and petrology of alkalic postshield and rejuvenated-stage lava from Kauai, Hawaii. Contrib. Mineral. Petrol. 99, 202–218.

Clague, D.A., Dixon, J.E., 2000. Environmental controls on the evolution of Hawaiian ocean volcanoes. Geochem. Geophys. Geosyst. (ISSN: 1525-2027) 1 (1999GC000023, 12 p.).

Clague, D.A., Frey, F.A., 1982. Petrology and trace element geochemistry of the Honolulu Volcanics, Oahu: implications for the oceanic mantle beneath Hawaii. J. Petrol. 23, 447–504.

Clague, D.A., Holcomb, R.T., Sinton, J.M., Detrick, R.S., Torresan, M.E., 1990. Pliocene and Pleistocene alkalic flood basalts on the seafloor north of the Hawaiian Islands. Earth Planet. Sci. Lett. 98, 175–191.

Clague, D.A., Moore, J.G., Dixon, J.E., Friesen, W.B., 1995. Petrology of submarine lavas from Kilauea's Puna Ridge, Hawaii. J. Petrol. 36, 299–349.

Clague, D.A., Moore, J.G., Davis, A.S., 2002. Volcanic breccia and hyaloclastite in blocks from the Nu'uanu and Wailau landslides, Hawaii. In: Takahashi, E., Lipman, P.W., Garcia, M.O., Naka, J., Aramaki, S. (Eds.), Hawaiian Volcanoes: Deep Underwater Perspectives. Geophysical Monograph, vol. 128, American Geophysical Union, Washington, pp. 279–296.

Clague, D.A., Davis, A.S., Dixon, J.E., 2003. Submarine strombolian eruptions along the Gorda mid-ocean ridge. In: White, J.D.L., Smellie, J.L., Clague, D.A. (Eds.), Explosive Subaequeous Volcanism. Geophysical Monograph, vol. 140, American Geophysical Union, Washington, pp. 11–128.

Cousens, B.L., 1996. Magmatic evolution of Quaternary mafic magmas at Long Valley Caldera and the Devil's Postpile, California: effects of crustal contamination on lithospheric mantle-derived magmas. J. Geophys. Res. 101, 26,673–27,689.

Dalrymple, G.B., Moore, J.G., 1968. ^{40}Ar excess in submarine pillow basalts from Kilauea Volcano, Hawaii. Science 161, 1132–1135.

Dartnell, P., Gardner, J.V., 1999. Sea-Floor Images and Data from Multibeam Surveys in San Francisco Bay, Southern California, Hawai'i, the Gulf of Mexico, and Lake Tahoe, California–Nevada. Digital Data Series DDS-55. U.S. Geol. Surv.

Davis, A.S., Clague, D.A., 2005. Deep submarine explosive basaltic eruptions at vents in the North Arch Volcanic Field. Bull. Volcanol. (14 p.). doi:10.1007/50045-005-008-7.

Davis, A.S., Clague, D.A., Friesen, W.F., 1994. Petrology and mineral chemistry of basalt from the Escanaba Trough, southern Gorda Ridge. U.S. Geol. Surv. Bull. 2022, 153–170.

Deino, A., Potts, R., 1990. Single-Crystal ^{40}Ar/^{39}Ar dating of the Olorgesailie Formation, Southern Kenya Rift. J. Geophys. Res. 95, 8453–8470.

Dixon, J.E., Clague, D.A., Wallace, P., Poreda, R., 1997. Volatiles in alkalic basalts from the North Arch volcanic field, Hawaii: extensive degassing of deep submarine-erupted alkalic series lavas. J. Petrol. 38, 911–939.

Doell, R.R., Dalrymple, G.B., 1973. Potasium–argon ages and paleomagnetism of the Waianae and Koolau volcanic series, Oahu, Hawaii. Geol. Soc. Am. Bull. 84, 1217–1242.

Duncan, R.A., Hogan, L.G., 1994. Radiometric dating of young MORB using ^{40}Ar/^{39}Ar incremental heating methods. Geophys. Res. Lett. 21, 1927–1930.

Feigenson, M.D., 1984. Geochemistry of Kauai volcanics and a mixing model for the origin of Hawaiian alkali basalts. Contrib. Mineral. Petrol. 87, 109–119.

Frey, F.A., 1980. The origin of pyroxenites and garnet pyroxenites from Salt lake Crater, Oahu, Hawaii: trace element evidence. Am. J. Sci. 280A, 427–449.

Frey, F.A., Garcia, M.O., Roden, M.F., 1994. Geochemical characteristics of Koolau Volcano: implications of intershield geochemical differences among Hawaiian volcanoes. Geochim. Cosmochim. Acta 58, 1441–1462.

Frey, F.A., Clague, D.A., Mahoney, J.J., Sinton, J.M., 2000. Volcanism at the edge of the Hawaiian plume: petrogenesis of submarine alkalic lavas from the North Arch volcanic field. J. Petrol. 41, 667–691.

Funkhouser, J.G., Barnes, I.L., Naughton, J.J., 1968. The determination of a series of ages of Hawaiian volcanoes by the potassium–argon method. Pac. Sci. 22, 369–372.

Gramlich, J.W., Lewis, V.A., Naughton, J.J., 1972. Potassium–argon dating of Holocene basalts of the Honolulu Volcanic series. Geol. Soc. Am. Bull. 82, 1399–1404.

Haskins, E.H., Garcia, M.O., 2004. Scientific drilling reveals geochemical heterogeneity within the Ko'olau shield, Hawai'i. Contrib. Mineral. Petrol. 17, 162–188.

Hauri, E.H., Lassiter, J.C., DePaolo, D.J., 1996. Osmium isotope systematics of drilled lavas from Mauna Loa, Hawaii. J. Geophys. Res. 101, 11,793–11,808.

Hay, R.L., Iijima, A., 1968. Nature and origin of palagonite tuffs of the Honolulu group on Oahu, Hawaii. Mem. Geol. Soc. Am. 116, 371–376.

Hay, R.L., Sheppard, R.A., 1977. Zeolites in open hydrologic systems. Mineralogy and Geology of Natural Zeolites, Short Course Notes, vol. 4. Mineral. Soc. Am., Washington, D.C., pp. 93–102.

Helz, R.T., 1987. Differentiation behavior of Iki lava lake, Kilauea Volcano, Hawaii: an overview of past and current work. In: Mysen, B.O. (Ed.), Magmatic Processes; Physicochemical Principles. Geochem. Soc. Spec. Pub., vol. 1, pp. 241–258.

Helz, R.T., Thornber, C.R., 1987. Geothermometry of Kilauea Iki lava lake, Kilauea Volcano. Bull. Volcanol. 49, 651–668.

Jackson, E.D., Wright, T.L., 1970. Xenoliths in the Honolulu volcanic series, Hawaii. J. Petrol. 11, 405–430.

Jackson, M.C., Frey, F.A., Garcia, M.O., Wilmoth, R.A., 1999. Geology and geochemistry of basaltic lava flows and dikes from the trans-Koolau tunnel, Oahu, Hawaii. Bull. Volcanol. 60, 381–401.

Lanphere, M.A., Dalrymple, G.B., 1980. Age and strontium isotopic composition of the Honolulu volcanic series, Oahu, Hawaii. Am. J. Sci. 280A, 736–751.

Lassiter, J.C., Hauri, E.H., 1998. Osmium isotope variations in Hawaiian lavas: evidence for recycled oceanic lithosphere in the Hawaiian plume. Earth Planet. Sci. Lett. 164, 483–496.

Lo, C.-H., Onstott, T.C., 1989. ^{39}Ar recoil artifacts in chloritized biotite. Geochim. Cosmochim. Acta 53, 2697–2711.

Maaloe, S., James, D., Smedley, P., Petersen, S., Garmann, L.B., 1992. The Kloa volcanic suite of Kauai, Hawaii. J. Petrol. 33, 761–784.

McDougall, I., 1964. Potassium–argon ages from lavas of the Hawaiian Islands. Geol. Soc. Am. Bull. 75, 107–128.

Moberly, R., Walker, G.P.L., 1987. Coastal and volcanic geology of the Hanauma Bay area, Oahu, Hawaii. Geol. Soc. Am. Cent. Field Guide, Cordilleran Section, pp. 5–10.

Moore, J.G., 1987. Subsidence of the Hawaiian Ridge. U.S. Geol. Surv. Prof. Pap. 1350, 85–100.

Moore, J.G., Fornari, D.J., Clague, D.A., 1985. Basalts from the 1877 submarine eruption of Mauna Loa, Hawaii: New data on the variation of palagonitization rate with temperature. U.S. Geol. Surv. Bull. 1663, 11 pp.

Montierth, C., Johnston, A.D., Cashman, K.V., 1995. An empirical glass-composition-based geothermometer for Mauna Loa lavas. Am. Geophys. Union Monogr. 92, 207–217.

Ozawa, A., Tagami, T., Garcia, M.O., 2005. Unspiked dating of the Honolulu rejuvenated and Ko'olau shield volcanism on O'ahu, Hawai'i. Earth Planet. Sci. Lett. 232, 1–11.

Reiners, P.W., Nelson, B.K., 1998. Temporal–compositional–isotopic trends in rejuvenated-stage magmas of Kauai, Hawaii, and implications for mantle melting processes. Geochim. Cosmochim. Acta 62, 2347–2368.

Roden, M.F., Frey, F.A., Clague, D.A., 1984. Geochemistry of tholeiitic and alkalic lavas from the Koolau range, Oahu, Hawaii: implications for Hawaiian volcanism. Earth Planet. Sci. Lett. 69, 141–158.

Samson, S.D., Alexander Jr., E.C., 1987. Calibration of the interlaboratory $^{40}Ar/^{39}Ar$ dating standard, Mmhb-1. Chem. Geol. 66, 27–34.

Sen, G., 1988. Petrogenesis of spinel lherzolite and pyroxenite suite xenoliths from the Koolau shield, Oahu, Hawaii: implications for petrology of the post-eruptive lithosphere beneath Oahu. Contrib. Mineral. Petrol. 100, 61–91.

Sen, G., Leeman, W.P., 1991. Iron-rich lherzolitic xenoliths from Oahu: origin and implications for Hawaiian magma sources. Earth Planet. Sci. Lett. 102, 45–57.

Sen, G., Macfarlane, A., Srimal, N., 1996. Significance of rare hydrous alkaline melts in Hawaiian xenoliths. Contrib. Mineral. Petrol. 122, 415–427.

Shinozaki, K., Ren, Z.-Y., Takahashi, E., 2002. Geochemical and petrological characteristics of Nuuanu and Wailau landslide blocks. In: Takahashi, E., Lipman, P.W., Garcia, M.O., Naka, J., Aramaki, S. (Eds.), Hawaiian Volcanoes: Deep Underwater Perspectives. Geophysical Monograph, vol. 128, American Geophysical Union, Washington, D.C., pp. 297–310.

Sisson, T.W., Lipman, P.W., Naka, J., 2002. Submarine alkalic through tholeiitic shield-stage development of Kilauea Volcano, Hawaii. In: Takahashi, E., Lipman, P.W., Garcia, M.O., Naka, J., Aramaki, S. (Eds.), Hawaiian Volcanoes: Deep Underwater Perspectives. Geophysical Monograph, vol. 128, American Geophysical Union, Washington, D.C., pp. 193–219.

Sobolev, A.V., Hofmann, A.W., Nikogosian, I.K., 2000. Recycled ocean crust observed in "ghost plagioclase" within the source of Mauna Loa lavas. Nature 404, 986–990.

Stearns, H.T., 1940. Supplement to the Geology and Groundwater Resources of the Island of Oahu, Hawaii. Bull., vol. 5, Hawaii Div. Hydrography, Wailuku, Maui. 164 pp.

Stearns, H.T., Dalrymple, G.B., 1978. The K–Ar age of the Black Point dike on Oahu, Hawaii, and its relation to the Yarmouth Interglaciation. Occas. Pap. Bernice P. Bishop Mus. 24, 307–313.

Stearns, H.T., Vaksvik, K., 1935. Geology and Groundwater Resources of Oahu, Hawaii. Bull., vol. 1. Hawai'i Div. Hydrography, Wailuku, Maui, 479 pp.

Stearns, H.T., Vaksvik, K., 1938. Records of the Drilled Wells on Oahu, Hawaii. Bull., vol. 4. Hawaii Div. Hydrography, Wailuku, Maui. 213 pp.

Steiger, R.H., Jäger, E., 1977. Subcommission on geochronology: convention on the use of decay constants in geo- and cosmochronology. Earth Planet. Sci. Lett. 36, 359–362.

Stille, P., Unruh, D.M., Tatsumoto, M., 1983. Pb, Sr, Nd, and Hf isotopic evidence of multiple sources for O'ahu, Hawai'i basalts. Nature 304, 25–29.

Sun, S.-s., 1980. Lead isotopic study of young volcanic rocks from mid-ocean ridges, ocean islands, and island arcs. Philos. Trans. R. Soc. London 297, 409–445.

Sun, S.-s., McDonough, 1989. Chemical and isotopic systematics of oceanic basalts: implications for mantle composition and processes. In: Saunders, A.D., Norry, M.J. (Eds.), Magmatism in the Ocean Basins. Geol. Soc. Spec. Pub., vol. 42, pp. 313–345.

Tanaka, R., Nakamura, E., 2002. Geochemical evolution of Koolau Volcano, Hawaii. In: Takahashi, E., Lipman, P.W., Garcia, M.O., Naka, J., Aramaki, S. (Eds.), Hawaiian Volcanoes: Deep Underwater Perspectives. Geophysical Monograph, vol. 128, American Geophysical Union, Washington, D.C., pp. 311–332.

Taylor, J.R., 1982. An Introduction to Error Analysis: the Study of Uncertainties in Physical Measurements. Univ. Sci. Books, Mill Valley, Calif, 270 pp.

Todt, A., Cliff, W.R., Hanser, A., Hofmann, A.W., 1984. ^{202}Pb–^{205}Pb spike for Pb isotopic analysis. Terra Cogn. 4, 209.

Wentworth, C.K., 1926. Pyroclastic geology of Oahu. Bernice P Bishop Mus. Bull. 30, 121 pp.

Winchell, H., 1947. Honolulu series, Oahu, Hawaii. Geol. Soc. Am. Bull. 58, 1–48.

Yang, H.-J., Frey, F.A., Clague, D.A., 2003. Constraints on the source components of lavas forming the Hawaiian North arch and Honolulu Volcanics. J. Petrol. 44, 603–627.

York, D., 1969. Least squares fitting of a straight line with correlated errors. Earth Planet. Sci. Lett. 5, 320–324.